Reduction of Ag+ irreversibly adsorbed on cyanide-modified Pt(111)

Jonathan A. Mwanda, Angel Cuesta

PII: S1572-6657(21)00065-5

DOI: https://doi.org/10.1016/j.jelechem.2021.115039

Reference: JEAC 115039

To appear in: *Journal of Electroanalytical Chemistry*

Received date: 14 September 2020

Revised date: 13 January 2021

Accepted date: 21 January 2021

Please cite this article as: J.A. Mwanda and A. Cuesta, Reduction of Ag+ irreversibly adsorbed on cyanide-modified Pt(111), *Journal of Electroanalytical Chemistry* (2021), https://doi.org/10.1016/j.jelechem.2021.115039

Reduction of Ag^+ irreversibly adsorbed on cyanide-modified Pt(111)

Jonathan A. Mwanda†, Angel Cuesta*
Department of Chemistry, School of Natural and Computing Sciences, University of Aberdeen, AB24 3UE, Scotland, UK
†Current address: Gulf Organization for Research and Development, Doha, Qatar
*Corresponding author: angel.cuestaciscar@abdn.ac.uk

ABSTRACT
We report a study of the electrochemical reduction of Ag^+ immobilized on a cyanide modified Pt(111) electrode in a Ag^+-free solution using cyclic voltammetry and in-situ STM. We show that, upon reduction at 0.29 V, Ag deposits directly on the platinum substrate, resulting in the formation of an AgPt surface alloy without loss of the cyanide adlayer The large affinity of Ag^+ for CN_{ad} is responsible for this large negative shift of the Ag^+/Ag redox couple.. A fraction of the electrodeposited Ag is reoxidised at 0.34 V to yield again Ag^+ coordinated to the CN adlayer. Therefore, successive cycling with a positive limit below 0.90 V results in a roughening of the surface and in the gradual transformation of cyanide-modified Pt(111) to a cyanide-modified AgPt surface alloy on Pt(111).
Keywords: Cyclic voltammetry; STM; electroreduction; Metallization; cyanide-modified Pt(111); Surface alloy

1 Introduction

Initial attempts to metallize molecular adlayers electrochemically (a particularly attractive method due to the low cost and simplicity of the equipment required) failed [1–6], with the deposited metal effectively creeping underneath and depositing on the metal substrate. In 2004 however, Kolb et al. [7] demonstrated the successful electrochemical metallization of a molecular adlayer via the immobilization of a metal cation on a self assembled monolayer (SAM) of an adequately functionalised molecule, followed by reduction in a metal free solution. Various groups have since demonstrated the metallization of SAMs employing electrochemical reduction techniques [8–11], although yielding 3D islands instead of the 2D islands reported by Kolb et al. [7,12,13]. For a recent review on this subject see [14].

The metallization of a SAM with an ordered array of metal islands of the same size would lead to a high density of molecular contacts per unit area, all with the same number of molecules sandwiched between the bidimensional metal island and the metallic substrate. In addition to the high density of circuit elements per unit area, such ordered array could have interesting properties associated to plasmon excitations or collective phenomena. Achieving this goal would require a nanopatterned SAM with an ordered distribution of equivalent adsorption sites, and a way to limit the diffusion of pre-adsorbed metal ions, thus limiting the aggregation and migration over the SAM of the bidimensional metal islands during and after the reduction step. We have attempted to reach this goal (unfortunately without success until now) by metallizing cyanide-modified Pt(111) electrodes using Kolb's method.

Cyanide adsorbs spontaneously and irreversibly on Pt(111), with the carbon end bonded linearly on-top of a platinum atom and the nitrogen end pointing into the solution, forming a (2√3 x 2√3) *R*30° structure [15–17]. We have shown that alkaline-metal cations [18–20], Cu^{2+} [19,21,22] and Pd^{2+} [23] adsorb on the cyanide adlayer due to the electrostatic interaction of the cation with the negative end of the dipole

of adsorbed cyanide, this adsorption being irreversible in the case of Cu^{2+} [19,21,22] and Pd^{2+} [23]. In-situ STM images of cyanide-modified Pt(111) electrodes in solutions containing Na^+, K^+, Cs^+ or Cu^{2+}, as well as of cyanide-modified Pt(111) electrodes with pre-adsorbed Cu^{2+} or Pd^{2+} in solutions free of the corresponding cation, show in all cases the formation of a honeycomb pattern, suggesting the adsorption of the cations around the CN rings at sites in which the cation interacts with the N atom of three CN groups [18,20–23].

Attempts to reduce the immobilised Cu^{2+} in Cu^{2+}-containing solutions failed to metallize the adlayer, resulting in the direct deposition of Cu onto the Pt substrate [21]. However, bidimensional Cu nanoislands were formed on the cyanide adlayer when Kolb's method was employed [22]. These islands were shown to deposit and dissolve reversibly, and to grow via an Ostwald's ripening process. Differences observed attempting to metallize the cyanide with Cu [22] and Pd [23] suggest that the interaction of the metal with the SAM might play an important role in determining the result of the electrodeposition process. In this work, we report on the attempt to metallize the cyanide adlayer on cyanide-modified Pt(111) electrodes by reducing Ag^+ ions immobilised on the cyanide SAM in Ag^+-free sulphuric acid solutions.

2 Experimental

The working electrode used for cyclic voltammetry (CV) was a bead type platinum single crystal (2 mm diameter) prepared according to the method developed by Clavilier et al. [24], oriented and polished parallel to the (111) plane (miscut < 0.05°). For electrochemical scanning tunnelling microscopy (EC-STM) experiments, the Pt(111) electrode used was a single-crystal disc (10 mm in diameter) purchased from MaTeck (Jülich, Germany, miscut < 1°). Before every experiment, the electrodes were flame annealed in a Bunsen burner and cooled in a H_2/N_2 reductive atmosphere. Once cold, a drop of Milli-Q water (18 MΩ cm, 2 ppb TOC) saturated with the cooling N_2 and H_2 mixture was attached to the exposed (111) surface in order to protect it during transport through the laboratory's atmosphere.

Cyanide-modified Pt(111) electrodes were prepared by immersing, immediately after the step described above, a clean and well-ordered Pt(111) electrode in a 0.1 M KCN (Merck, pa) solution for approximately 3 min, after which the electrode was rinsed with ultrapure water. Pre-adsorption of Ag^+ was achieved by immersing the cyanide-modified Pt(111) electrode in 0.1 M $HClO_4$ + 1 mM $AgClO_4$ for approximately 3 min, followed by rinsing with Milli-Q water. All the experiments were carried out in Ag^+-free 0.1 M H_2SO_4. Solutions were prepared from concentrated H_2SO_4 (Merck, Suprapur) and $AgClO_4 \cdot H_2O$ (Sigma Aldrich, 99.99% trace metal analysis). All CVs were measured after degassing the solution with N_2 (BOC, Research Grade N5.5).

Platinum wires (Alfa Aesar 99.997%, 0.5 mm in diameter) were utilized as auxiliary electrodes. A reversible hydrogen electrode (RHE) and a Pt wire were used as reference and quasi-reference electrode, respectively, for CV and EC-STM, respectively. All potentials in the text are referred to the RHE scale, unless otherwise stated.

STM images were recorded using a PicoLe Molecular Imaging with a PicoScan 2100 controller. Tungsten tips for STM experiments were etched from a polycrystalline W wire (0.25 mm in diameter) in 2 M NaOH and coated with electrophoretic paint to minimize the faradaic current at the tip/electrolyte interface. All images were acquired in the constant-current mode.

3 Results and Discussion

3.1 Cyclic Voltammetry

Cyanide-modified Pt(111) electrodes with pre-adsorbed Ag^+ were immersed in Ag^+-free 0.1 M H_2SO_4 at 0.80 V, and a CV at 0.05 V s^{-1} was then started with a potential sweep in the negative direction. The first and second CVs are shown in Fig. 1, solid and dotted black lines respectively. The CV of the same electrode if, after immersion in the same electrolyte, cycling is kept within the potential region between 0.6 and 1.10 V, as well as that of a cyanide-modified Pt(111) in 0.1 M H_2SO_4 without pre-adsorbed Ag^+ (red line), are also shown for comparison.

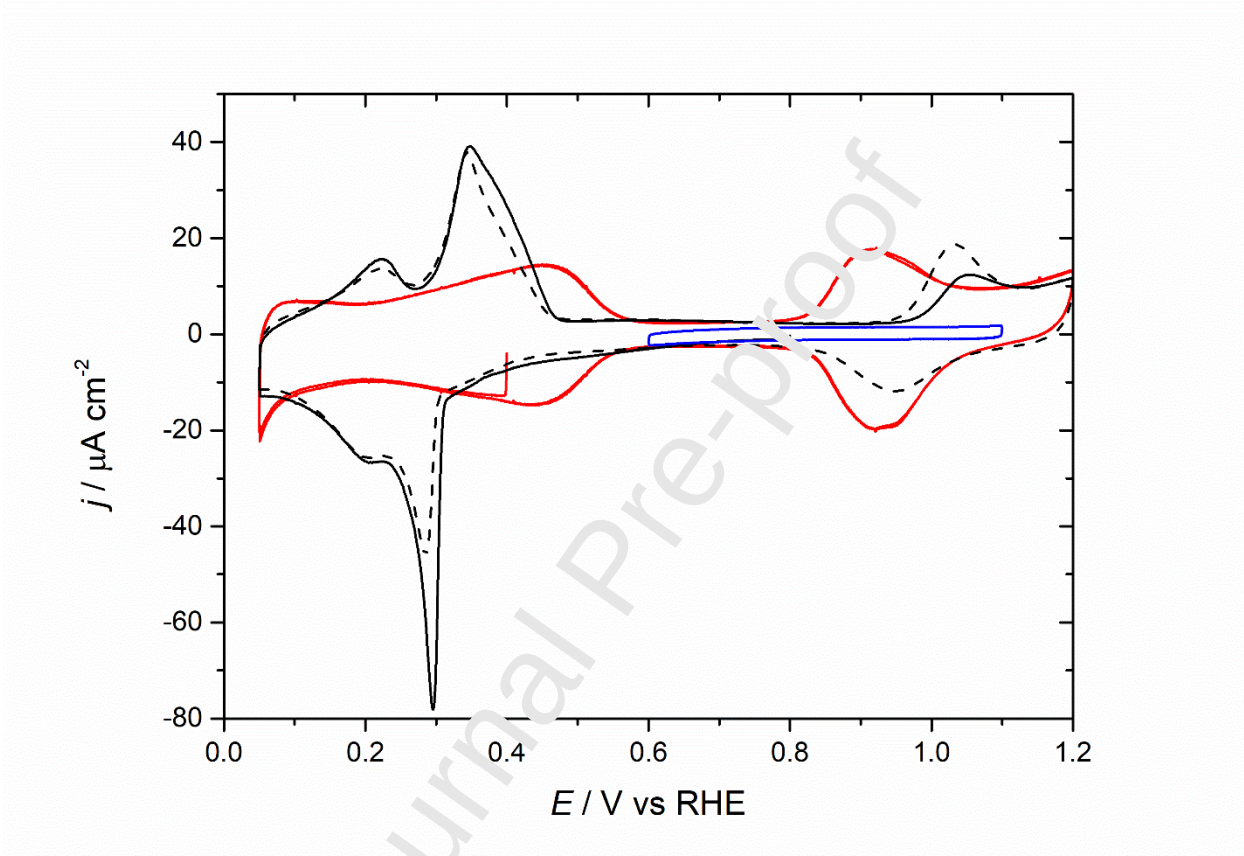

Figure 1. First (solid black line) and second (dotted line) cyclic voltammograms in Ag^+-free 0.1 M H_2SO_4 of a cyanide-modified Pt(111) electrode on which Ag^+ had been pre-adsorbed. The blue line corresponds to the cyclic voltammogram of the same electrode in the same solution if the negative potential limit is kept above 0.6 V, thereby preventing the reduction of pre-adsorbed Ag^+. The red line corresponds to the cyclic voltammogram of a cyanide-modified Pt(111) electrode without pre-adsorbed Ag^+ in the same electrolyte. Scan rate: 0.05 V s^{-1}.

The CV of cyanide-modified Pt(111) (red line) is characterized by a broad reversible feature between 0.05 and 0.50 V, corresponding to a proton-electron transfer to CN_{ad} to form $(CN)_xH_{ad}$, with x decreasing with increasingly negative potential [18]. We have previously demonstrated that M^{z+} cations can interact electrostatically with the negative partial charge on the nitrogen atom of CN_{ad}, and that, depending on the cation, this can result either in the reversible adsorption of the cation on the cyanide-modified Pt(111) surface [20,25], or in irreversible adsorption [22,23]. In all cases, adsorption of M^{z+} on cyanide-modified Pt(111) results in a negative shift of the onset of hydrogen adsorption, due to the competition between M^{z+} and H^+ for the same adsorption sites on the cyanide adlayer. This is also observed in Fig. 1, providing evidence of the irreversible complexation of Ag^+ with CN_{ad}.

A second surface process appears just above 0.90 V in the CV of cyanide-modified Pt(111) which, although still not clearly identified, have been associated with the adsorption of oxygenated species such as OH [26,27]. In the presence of pre-adsorbed Ag^+, this process is completely blocked as long as the negative potential limit is kept more positive than 0.60 V (Figure 1, blue line), thereby preventing the reduction of pre-adsorbed Ag^+. This suggests either that (i) the adsorption process around 0.90 V involves the nitrogen atoms of the CN_{ad} groups, which are blocked by pre-adsorbed Ag^+ or (ii) pre-adsorbed Ag^+ ions prevent the access of water molecules to the surface of the Pt(111), inhibiting the formation of OH_{ad} on Pt.

If the negative potential limit is extended below 0.60 V, a new reduction peak emerges in the first negative sweep at 0.29 V (Figure 1, black solid line). The corresponding anodic counterpart appears as an asymmetric peak at 0.34 V. It is reasonable to attribute the cathodic peak at 0.29 V to the reduction of Ag^+ coordinated to CN_{ad} to Ag, and the peak at 0.34 V to the reverse process:

$$\mathrm{CN_{ad}} - \mathrm{Ag^+} + \mathrm{e^-} \rightleftharpoons \mathrm{Ag} + \mathrm{CN_{ad}} \quad (1)$$

Please note that this is much more negative than the standard equilibrium potential for the Ag^+/Ag couple (0.86 V *vs.* RHE at this pH), therefore, the anodic peak at 0.34 V cannot correspond to the oxidation of Ag to aqueous Ag^+. However, oxidation of Ag at this potential is still possible if the final state is Ag^+ coordinated to CN_{ad} due to the strong interaction of Ag^+ with CN_{ad} (otherwise adsorption of Ag^+ on cyanide-modified Pt(111) would not be irreversible). This results in a considerable stabilization of the oxidised form of this couple (CN_{ad}–Ag^+) which contributes to the significant negative shift of the corresponding equilibrium potential. The same peak, a bit less intense, appears in the second negative sweep (Figure 1, dotted black line). The difference between the charge density in the first and second negative sweeps amounts to ca. 17.0 μC cm^{-2}, suggesting that less CN_{ad} - attached Ag^+ is available for reduction to Ag in the second sweep. We will discuss this in more depth below.

A reversible process around 0.20 V appears immediately after the negative peak at 0.29 V. A similar reversible peak has been observed in the voltammetric profile of $AgPt_{1-x}$/Pt(111) surface alloys, and has been attributed to the adsorption of hydrogen on alloys with a Ag content higher than 50% [28,29]. This suggests that reduction of CN_{ad}-coordinated Ag^+ at 0.29 V results in the immediate formation of a surface AgPt alloy with a local content of Ag higher than 50%, and that the silver slowly disperses throughout the Pt(111) surface upon repeated cycling.

Following the reduction processes described above, the surface process observed around 0.90 V in the CV of cyanide-modified Pt(111) (see Fig. 1, red line) re-emerges after the first negative potential excursion, but now at a slightly more positive potential around 1.0 V. This peak at ca. 1.0 V appears less symmetrical and slightly more positive than the peaks around 0.9 V on cyanide-modified Pt(111) (see Fig. 1, red line). It is reasonable to also ascribe the new process to the adsorption of oxygenated species such as OH, as the peaks occurring around 0.9 V on the cyanide modified Pt(111) [26,27]. The positive shift and differing shape of the peaks is possibly due to OH adsorption on a cyanide-modified AgPt alloy, as opposed to cyanide-modified on Pt(111).

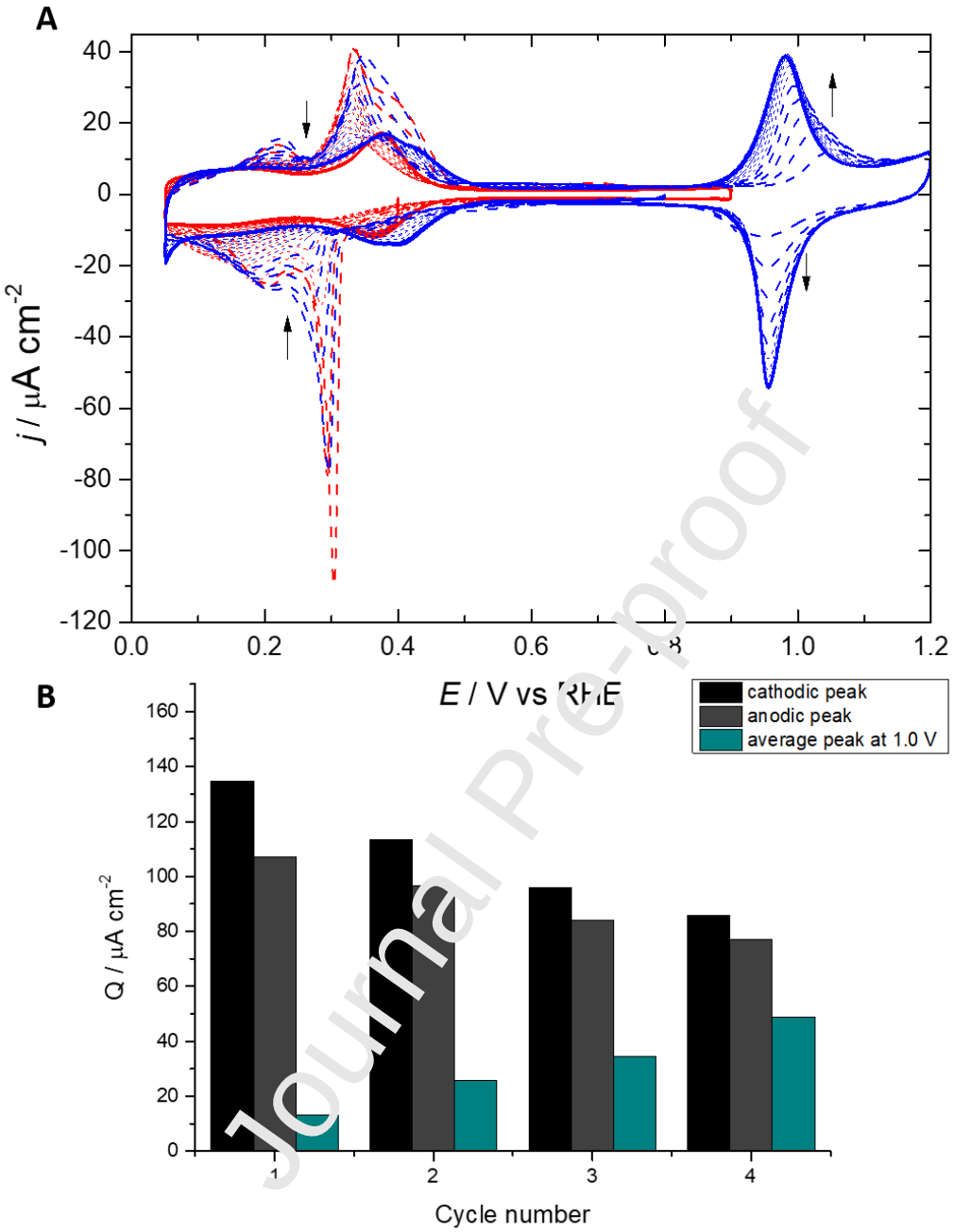

Figure 2. A: Evolution of the cyclic voltammogram in 0.1 M H_2SO_4 of a cyanide-modified Pt(111) electrode on which Ag^+ had been pre-adsorbed with successive cycling between 0.05 and 1.20 V (blue line) and between 0.05 and 0.9 V (red line) at a scan rate of 0.05 V s^{-1}. The blue and red solid lines indicate the final steady state, and the black arrows indicate the direction of evolution of the voltammetric profile. **B:** Bar graph showing the charge density obtained by integration of the CV between 0.1 and 0.5 V in the negative (black) and positive (grey) potential sweeps of the first four cycles. The horizontal red dashed lines highlight the clear correlation between the charge density in the cathodic sweep and that in the subsequent anodic sweep.

Fig. 2 A illustrates the evolution with successive cycling of the CV in 0.1 M H_2SO_4 of a cyanide-modified Pt(111) electrode on which Ag^+ had been pre-adsorbed. The first negative scan when the positive potential limit is set to 1.2 V (blue lines), overlaps with the first negative scan when the positive limit is 0.9 V (red lines) and therefore has not been included in the figure. Independently of the positive

potential limit, upon successive cycling the peaks at 0.29 (cathodic) and 0.34 (anodic) V attributed to the $Ag^+(CN_{ad})/Ag$ couple decrease in intensity. Similarly, the reversible process around 0.20 V, attributed to the adsorption of hydrogen on a surface AgPt alloy with a Ag local content higher than 50% continuously decreases in intensity, until its practical disappearance. Regarding the process around 1.0 V (obviously only observable when the potential limit is increased from 0.9 to 1.2 V), attributed to the adsorption of oxygenated species on the cyanide modified AgPt alloy, it becomes more reversible and increases in intensity with repeated cycling, mirroring the decrease in intensity of the processes at 0.29/0.34 V and around 0.20 V. The decrease of the charge density associated with the latter processes is illustrated in the bar chart in Fig. 2 B, which shows the double-layer corrected charge densities in the potential region between 0.1 and 0.5 V for the first four cycles. Double layer correction was done by assuming that the double-layer capacitance, as estimated from the current between 0.6 and 0.8 V, remains constant over the whole voltammetric potential range, and subtracting the charge density corresponding to that capacitance between 0.1 and 0.5 V from that resulting from integrating the CV within that potential region. (Please note that the current and the charge density in this region mainly corresponds to hydrogen adsorption on the cyanide adlayer and, upon eventual partial stripping of CNad, of Pt and PtAg alloy regions. The charge corresponding to silver deposition is relatively small and concentrated within the peak at approximately 0.30 V.)

The continuous decrease of the overall charge density in this potential region suggests a continuous decrease in the amount of pre-adsorbed Ag^+ ions coordinated to CN_{ad} available for reduction. Of interest is the good match between the anodic charge density in a given cycle and the cathodic charge density in the subsequent cycle, as highlighted by the red dashed lines in Fig. 2 B. This suggests that the amount of Ag^+ reduced in cycle $n + 1$ corresponds to the fraction of Ag^+ produced by oxidation of Ag in the surface AgPt alloy in cycle n that had re-adsorbed on the CN_{ad}, thus confirming our assignment of the process at 0.29/0.34V to the $Ag^+(CN_{ad})/Ag$ redox couple.

The reduction in the charge density associated to the redox process at 0.29/0.34 V is accompanied by a decrease in the reversible peaks occurring at ca. 0.20 V (Fig. 2 A). This decrease suggests that, although the total amount of Ag in the AgPt surface alloy increases with cycling, the dilution of Ag in the alloy also increases. This apparent contradiction can be explained by considering that the presence of the reversible process at 0.20 V characteristic of $Ag_xPt_{1-x}/Pt(111)$ surface alloys with more than 50% will be determined by the local concentration of Ag. Initially, the alloy forms only on those regions where silver penetrates the cyanide adlayer and, although the total amount of Ag deposited is small, it results in a high local concentration above 50%. The maximum amount of Ag^+ that can be adsorbed on CN_{ad} in the honeycomb structure amounts to 0.16 ML [18,20,22,23] thus the overall concentration of Ag in the alloy can never approach 50%. During cycling, the mobility of Ag within the surface decreases the inhomogeneity in the local Ag concentration and the local Ag concentration of the surface alloy slowly approaches the overall Ag concentration, with a limiting value of 0.16 ML, thus explaining the continuous decrease in the reversible peaks around 0.20 V.

From previous work by our group [27] and others [30], we know that oxidative stripping of adsorbed cyanide starts above 1.1 V. The differences between the final, steady state voltammogram, when positive scan limits of either 0.90 V (Fig. 2A, red-dashed lines) or 1.2 V (Fig. 2 A blue-dashed lines) are used can be attributed, therefore, to the disruption of the cyanide layer above 1.1 V. The main difference is observed in the region between 0.05 and 0.5 V, in which the charge density is 17.2 $\mu C\ cm^{-2}$ for the more positive potential limit. As shown by Huerta et al. [31], this extra charge must correspond to sulphate adsorption within the cyanide-free Pt(111) patches left free upon partial stripping of the cyanide adlayer.

The evolution of the peaks just below 1 V with successive cycling is the result from several contributions. Although PtAg surface alloys do not show any voltammetric peak in this region [28] (and therefore, these peaks cannot be attributed to the oxidation-reduction of the PtAg surface), dissolution of Ag from the surface alloy has been demonstrated to start around 0.95 V [29] and must contribute to this current, particularly in the first cycles. This is confirmed by the roughening of the electrode surface in this potential region as revealed by in-situ STM (see below). Peaks in this potential region are also absent on a naked Pt(111) surface, but emerge upon cyanide adsorption and increase in intensity with increasing cyanide coverage [31]. However, even for the highest possible cyanide coverage the peaks are not as sharp as in Fig. 2A (see, e.g., the CV of cyanide-modified Pt(111) in Fig. 1, red line). Based on these arguments, we assign the reversible peaks around 1 V in the CV in Fig. 2A to the adsorption of OH on a rough PtAg surface alloy on Pt(111) covered by a perturbed cyanide adlayer. In the case of the CV with a positive scan limit of 1.2 V (blue line in Fig. 2A), the Ag content of the surface alloy and the cyanide coverage must be lower than when the potential limit is kept below 0.9 V, due to partial dissolution of Ag and partial stripping of the cyanide adlayer, respectively.

3.2 EC-STM

EC-STM was used to monitor the surface structure and morphology changes associated to the voltammetric features as described in the previous section.

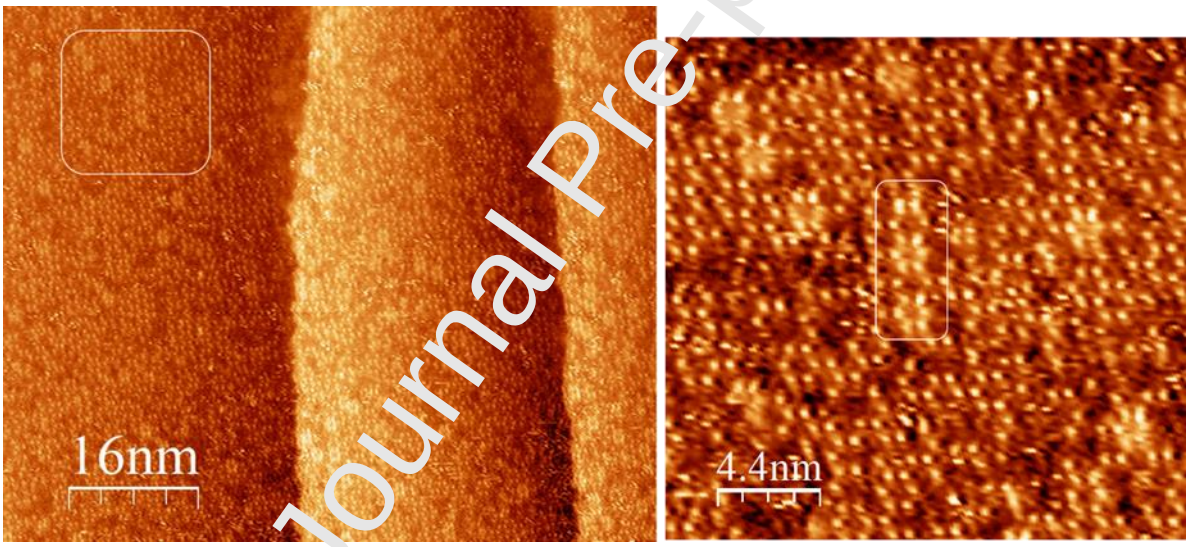

Figure 3. In-Situ STM images of a cyanide-modified Pt(111) on which Ag^+ had been pre-adsorbed in Ag^+-free 0.1 M H_2SO_4 at E= 0.80 V, U_T = 0.50 V (tip negative); I_T = 2 nA. The image in the left panel corresponds to an area 80 x 69 nm^2, while the right panel is a zoom in corresponding to the white square in the left panel (22 x 21 nm^2).

Fig. 3 shows STM images in Ag^+-free 0.1 M H_2SO_4 at 0.80 V of a cyanide modified Pt(111) electrode on which Ag^+ had been pre-adsorbed. Tunnelling maxima forming a honeycomb pattern cover the whole surface, but for some defects within the structure. Similar honeycomb structures have been observed by EC-STM upon irreversible adsorption of Cu^{2+} [22] on cyanide-modified Pt(111) electrodes, as well as on cyanide-modified Pt(111) electrodes immersed in acidic solutions containing Li^+, Na^+, K^+ or Cs^+ above a cation-specific threshold concentration [20]. A typical STM image of a cyanide modified Pt(111) without pre-adsorbed cations or in solutions containing Li^+, Na^+, K^+ or Cs^+ below their corresponding threshold concentration can be found in the supporting information to reference [20], and is identical to those reported decades ago by other groups for the (2√3 x 2√3) R30° structure of cyanide on Pt(111)

[16,32]. The honeycomb pattern observed in Fig. 3 is therefore also attributed in this case to non-covalently coordinated Ag^+ on the cyanide SAM.

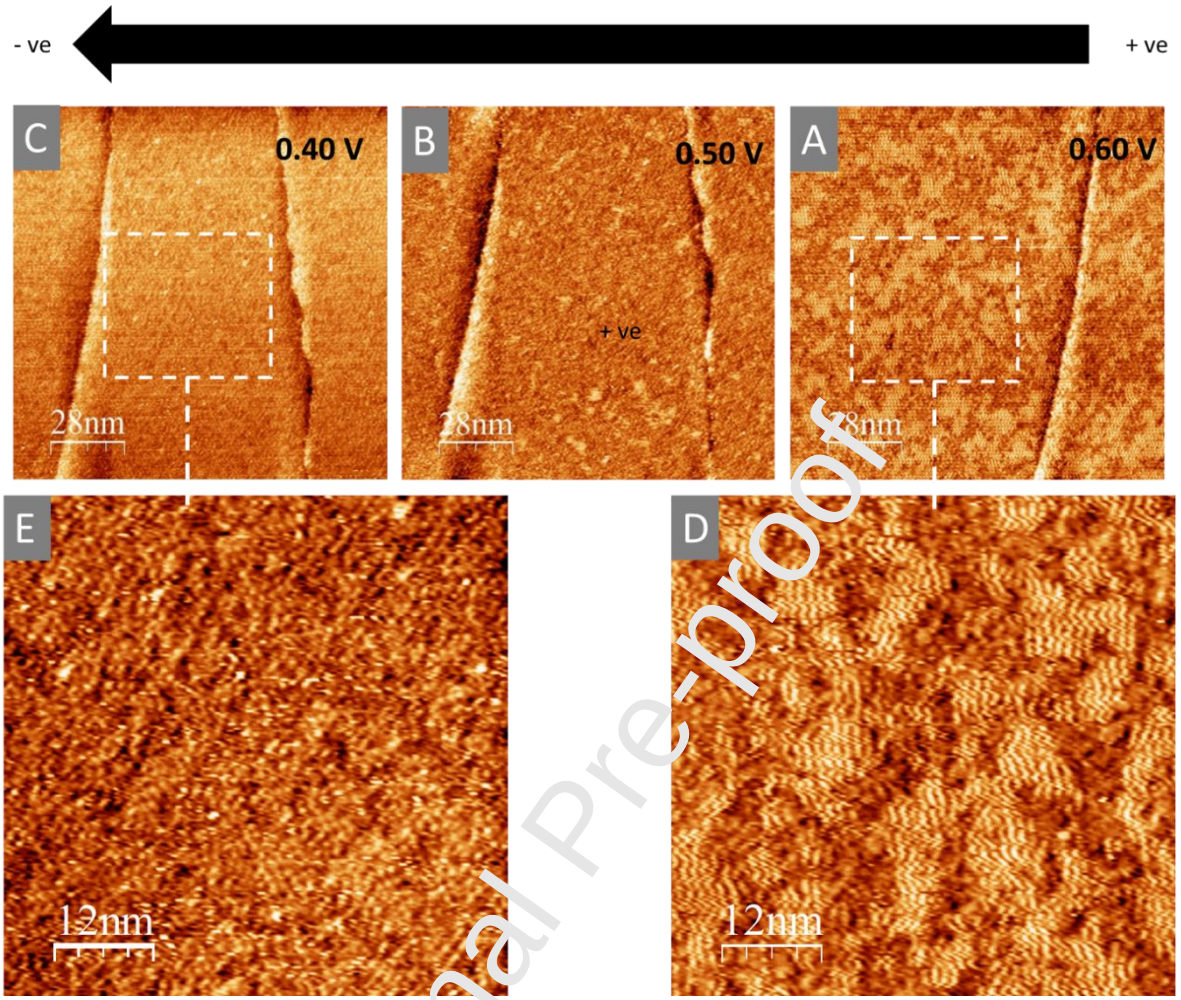

Figure 4. In-situ STM images (140 x 140 nm^2) recorded during the reduction of Ag^+ pre-adsorbed on a cyanide modified Pt(111) electrode in Ag^+-free 0.1 M H_2SO_4. Images recorded during the sequential reduction of the pre-adsorbed Ag^+, from left to right **(A)** E = 0.60 V, U_T = 0.40 V, **(B)** E = 0.50 V, U_T = 0.30 V, **(C)** E = 0.40 V, U_T = 0.20 V. Images (**D**) and (**E**) are 60 x 60 nm^2 zoom-ins corresponding to the dashed white squares in images **A** and **B**, respectively. All images acquired with tip negative biases and at I_T = 2 nA.

Figs. 4 A, B and C correspond to a series of STM images acquired sequentially from positive to more negative potentials (direction of black arrow) at 0.60, 0.50 and 0.40 V. At 0.60 V, the areas covered by the honeycomb structure observed at 0.80 V transform into high contrast areas containing zig zag lines running parallel to each other and separated by ca. 1 nm. This slight change is not accompanied by any voltammetric feature, which is most likely due to the slow rate of this process and the different time scales of the voltammetric and the STM experiments. As shown clearly in Fig. 4 D, the zigzag lines tend to align in three rotational domains rotated ca. 120° with respect to each other. The periodicity of the lines and the three rotational domains aligned with the substrate's main crystallographic directions suggest they correspond to edges of the hexagons formed by Ag^+ cations in the honeycomb structure on cyanide-modified Pt(111). The observation of edges rather than individual spots, like at 0.80 V, is attributed to an increased mobility leading to Ag^+ ions moving more easily among adsorption sites. In this scenario, the orientation of the line would indicate the direction along which the cations are moving when transiting among adsorption sites, thus explaining why only some of the edges of the hexagons

constituting the honeycomb can be observed. The reason behind the increased mobility of the Ag^+ ions in the honeycomb at this potentials and not more positive potentials is possibly connected to ion pairing with (bi)sulphate ions from the electrolyte, as discussed below.

A potential step from 0.60 to 0.50 V is accompanied by the vanishing of ca. 80% of the high contrast areas, which disappear completely (but reversibly if the potential is not stepped into the Ag deposition region) at 0.40 V. It is not very clear what is provoking this disappearance, as there is no feature in the CV in this potential region (see Fig. 1), but preliminary simulations of STM images using DFT suggest that, with the tunnelling biases employed, the density of states (DOS) of unoccupied energy levels on the cations coordinated to the cyanide adlayer at energies below the tip's Fermi level (allowing for tunnelling from the negatively biased tip to the cations) is zero and they should not be visible to STM, unless forming ionic pairs with oxyanions like sulphate or perchlorate, which leads to the emergence of empty DOS. Therefore, we provisionally attribute the apparent vanishing of the honeycomb features to the release of sulphate from these ionic pairs as the negative charge density on the Pt(111) substrate increases (at potentials more negative). We also suggest that partial release of sulphate in these ionic pairs is responsible for the increased mobility observed at 0.60 V and discussed in the paragraph above.

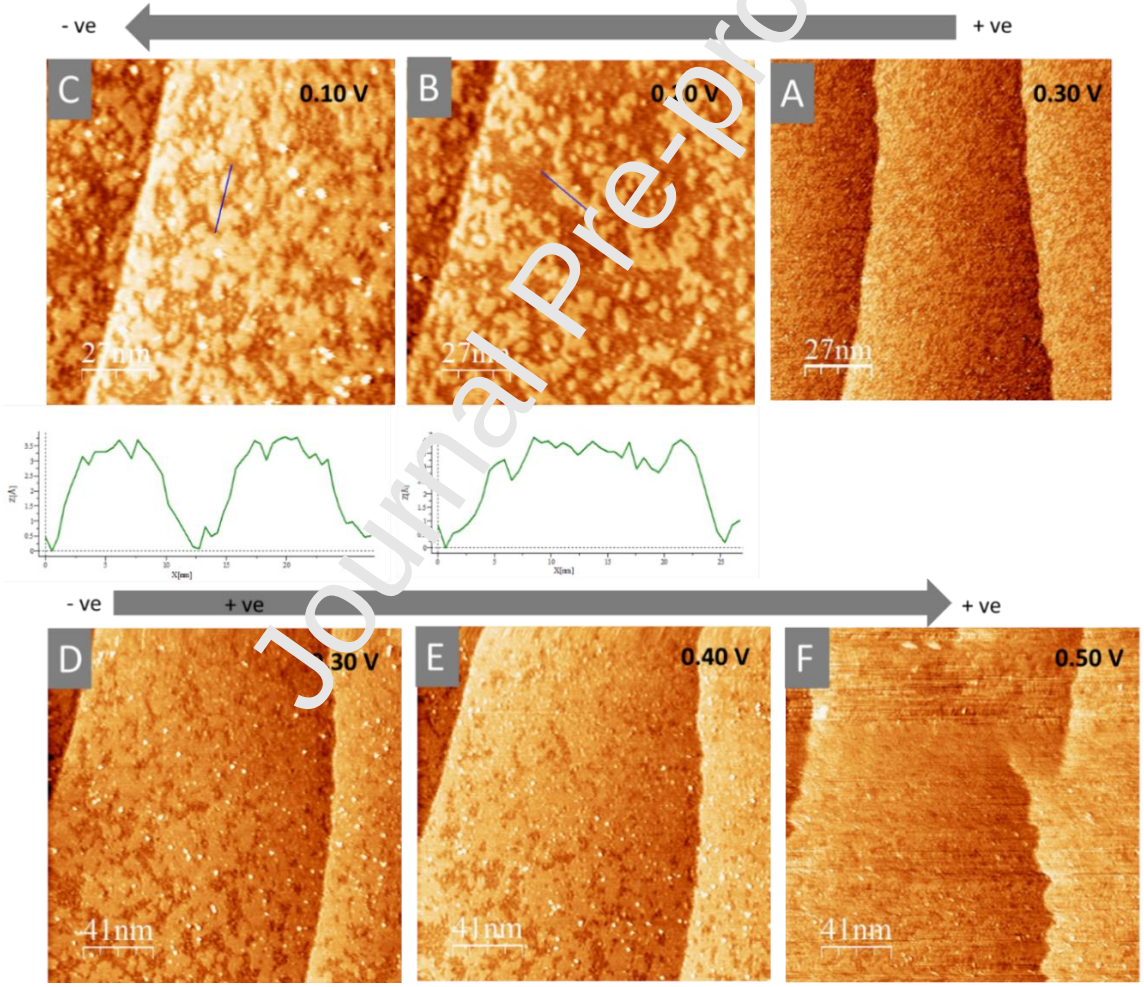

Figure 5. (A-C) In-situ STM images (135 x 135 nm^2) recorded during the sequential reduction of Ag^+ pre-adsorbed on cyanide-modified Pt(111) at E = 0.30 V (**A,** U_T = 0.10 V, tip negative), E = 0.20 V (**B**, U_T = 0.10 V, tip negative), and E = 0.10 V (**C**, U_T = 0.10 V, tip positive). **(D-F)** STM images (205 x 205 nm^2) recorded during the subsequent oxidation of the deposited Ag at E = 0.30 V (**D**, U_T = 0.10 V, tip negative), E = 0.40 V (**E**, U_T = 0.20 V, tip negative) and E = 0.50 V (**F**, U_T = 0.30 V, tip negative). All images acquired at tunnel current, I_T = 2 nA. The height profiles shown below images **(B)** and **(C)** correspond to those along the blue lines in the corresponding images.

Figs. 5 A, B and C illustrate images successively acquired in the direction of the arrow from positive to more negative potentials at 0.30, 0.20 and 0.10 V. The image at 0.30 V shows no significant change as compared with the image acquired at 0.40 V, except for an increased contrast of the atomic-scale features within the terrace, which we were unable to image with a higher resolution. However, at 0.20 V bidimensional islands with an apparent height of 0.4 nm emerge. These islands are spread across the terraces and step edges, with a slight preference for nucleation on the top side of monoatomic steps, and we attribute them to one-atom high heteroepitaxial islands of Ag on the Pt(111) substrate. While a height of ca. 0.30 nm would be expected, STM images are a convolution of both topography and local tunneling barrier, and the difference between the work functions of Ag and Pt contributes to the apparent increased height of the bidimensional Ag Islands. It is worth noting that the islands cover more than 16% of the surface, whereas the maximum possible coverage by Ag^+ in the honeycomb structure shown in Fig. 3 is 0.16 ML. Therefore, the bidimensional islands in Fig. 5 cannot correspond to pure Ag, whether on or underneath the cyanide adlayer.

At 0.10 V (Fig. 5 C), the surface coverage by the bidimensional islands increases, as does the interconnectivity between them. At the same time, the apparent height of the islands decreases to ca. 0.35 nm, closer to that expected from purely geometrical considerations. Considering that the coverage of Ag^+ coordinated on the CN_{ad} is at most 0.16 ML, a coverage of the Pt(111) by bidimensional Ag islands beyond that limit is not possible. The clearly higher coverage observed in Fig. 5 C at 0.10 V must therefore be due to the formation of a AgPt surface alloy and concomitant Pt enrichment. This is in agreement with the assignment of the peak at 0.20 V in the corresponding CV (see Fig. 1) to the adsorption of hydrogen on a AgPt alloy containing more than 50% Ag. The decrease in the apparent height from 0.4 nm at 0.20 V to 0.35 nm at 0.10 V is consistent with an increase of the Pt content in the surface alloy. The formation of the AgPt surface alloy in the hydrogen adsorption region, as well as the enrichment in Pt at the most negative potential, must be caused by the surface diffusion of Pt into the islands from the steps and from underneath the Ag islands (and the concomitant diffusion of Ag into the surface of Pt). The increased diffusion at more negative potentials might be the result of the stronger adsorption of hydrogen on Pt, as compared to Ag. Also observed in the image at 0.10 V in Fig. 5 C is the emergence of bright spots preferentially deposited on the AgPt alloy bidimensional islands that we attribute to Pt clusters 0.6 – 0.7 nm in height and composed of 4-5 atoms. The observation of similar clusters during AgPt alloy formation has been previously reported [28,29], and attributed to the very narrow miscibility region of Ag and Pt. The platinum clusters are generated by displacement from the surface and subsequent deposition onto the Ag islands. Due to the very strong bond between the Pt atoms on the surface and adsorbed cyanide, we find it unlikely that all these processes result in the stripping of the cyanide adlayer and suggest that the processes described above result in a PtAg surface alloy buried under the cyanide adlayer. This is consistent with the evolution of the voltammetric profile described in the previous section. As discussed there, only when the potential is scanned beyond 1.1 V partial oxidative stripping of CN_{ad} occurs.

Figs. 5 D-F show STM images acquired after Ag deposition and surface alloy formation at 0.1 V (see Fig. 5 D), with an arrow indicating the sequence of imaging from negative to positive potentials. A potential step from 0.10 V to 0.30 and then 0.40 V results in a decrease of contrast and an increase of the surface coverage by the higher contrast features. We attribute this to an increase of Pt concentration in the AgPt surface alloy as some Ag is dissolved and attached again as Ag^+ to the cyanide layer (see discussion on the voltammetric profile in section 3.1), leading to a more homogenous composition of the electrode surface. A significant change is observed upon excursion to 0.50 V (Fig. 5 F), which results in a fuzzy image with wavelike step edges. As discussed in the section 3.1, the peak at 0.34 V in the CV of Fig. 1

cannot correspond to dissolution of Ag as Ag^+ into the aqueous solution and is therefore attributed to the oxidation of Ag to yield Ag^+ coordinated on the cyanide adlayer. The noisy appearance of the image at 0.50 V (Fig. 5 F) can be explained by the high mobility of the Ag^+ ions coordinated to the cyanide adlayer at low coverage. Please note that, even with the higher initial coverage, the STM images become noisy around 0.50 V (Fig. 4), which we have attributed to an increased mobility of Ag^+ ions adsorbed on the cyanide adlayer due to the release at sufficiently negative potentials of sulphate in Ag^+-sulphate ion pairs.

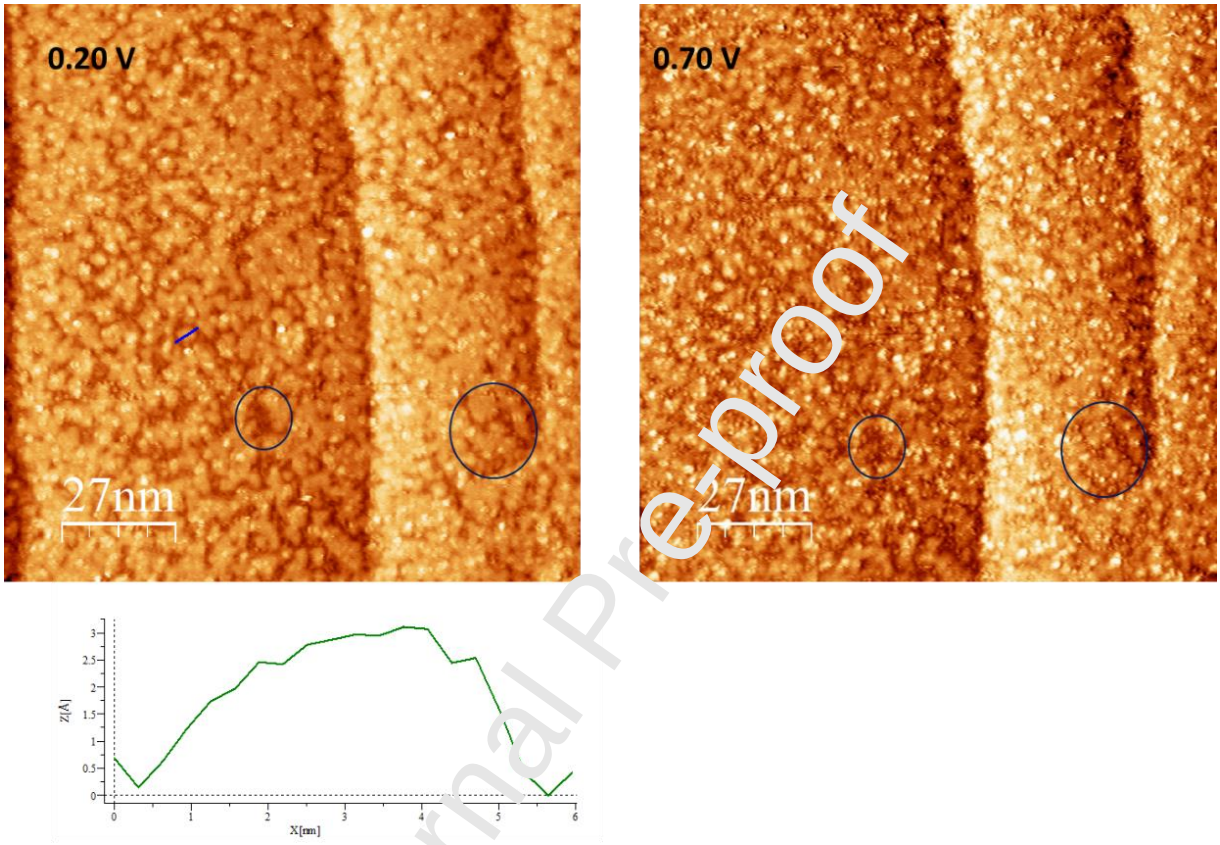

Figure 6. In situ STM images (135 x 135 nm^2) corresponding to the steady state achieved after repetitive potential cycling in Ag^+-free 0.1 M H_2SO_4. Left: at E = 0.20 V, (U_T = 0.50 V, tip negative); Right: at E = 0.70 V after a potential excursion to 1.0 V (U_T = 0.50 V, tip negative). Both images acquired at tunnelling current, I_T = 2 nA. The height profile on the left corresponds to the blue line across the island in the corresponding image. Blue circles of different sizes highlight the same areas in both images.

Fig. 6 shows STM images acquired once the steady-state CV has been obtained after repetitive cycling between 0.05 and 0.9 V. At 0.20 V the surface is covered by an interweaved pattern with an apparent height difference of 0.3 nm between high and low contrast areas, clearly smaller than that of similar features observed immediately after the first deposition of Ag (0.4 nm, see Fig. 5 C). As discussed above, we attribute the lower contrast to a lower Ag content in the AgPt surface alloy formed upon deposition. The interweaved pattern is due to the very narrow miscibility gap of Ag and Pt, which results in a tendency to phase separation into Pt- and Ag-rich areas, as observed in other surface alloy systems [33,34]. An image of the same area acquired at 0.70 V after excursion to 1.0 V shows that, although the contrast between brighter and darker areas has decreased, the shape of the features has barely changed at all (see, *e.g.*, blue circled areas in Fig. 6). There is also an increase in the number of small brighter spots, the height of which roughly corresponds to two atomic layers. This suggests that, even at the positive potential limit of the CV, part of the Ag in the surface alloy remains in the surface. A similar

behaviour has been reported by Beckord et al. during the dealloying of AgPt surface alloys [28], and was attributed to the strong lateral ligand effects contributed by the neighbouring Pt atoms, which results in the stabilization of the surface alloy.

In summary, successive potential cycling of Ag^+ preadsorbed on a cyanide modified Pt(111) results in Ag deposit on the Pt substrate. The Ag deposit forms a AgPt surface alloy at potentials negative of 0.2 V. Partial reoxidation of some of the Ag in the surface alloy to yield Ag^+ adsorbed on the remaining cyanide adlayer is observed at 0.34 V. As only part of the deposited Ag is oxidized in this process, the corresponding charge density diminishes with successive potential cycling. When the positive potential limit is extended to 1.2 V, some of the Ag is released as Ag^+ into the bulk of the solution and the cyanide adlayer is partially stripped. In comparison, repeated potential cycling for long periods of a polycrystalline platinum in a Ag^+-containing solution also results in the formation of an AgPt alloy [35]. In the case of Pt(111) in Ag^+ containing solution, a layer by layer growth of Ag deposition followed by formation of Ag clusters has been reported [36,37]. The Ag clusters have been demonstrated to subsequently form an AgPt alloy upon annealing at 620 K [36]. This is in contrast with our observation of AgPt surface alloy formation on Pt(111) upon repeated potential cycling in a solution containing no Ag^+ and at room temperature.

4 Conclusion

We have attempted the metallization of cyanide-modified Pt(111) electrodes by reducing pre-adsorbed Ag^+ in Ag^+-free sulphuric acid. By combining cyclic voltammetry and in-situ STM, we have shown that, above 0.70 V, Ag^+ adsorbs irreversibly on the cyanide adlayer forming a honeycomb structure, similar to that previously reported with preadsorbed Cu^{2+} [22], as well as in solutions containing alkaline-metal cations [20]. We have also shown that reduction of the pre-adsorbed Ag^+ ions results in the deposition of Ag on the Pt(111) substrate. This reduction, and the subsequent reoxidation to yield Ag^+ coordinated to CN_{ad}, occurs at a potential much more negative than expected from the standard potential of the Ag^+/Ag couple, which can be attributed to the increased stability of the oxidized form of the couple due to its interaction with CN_{ad}.

Ag deposition is followed by the formation of AgPt surface alloy. The formation of AgPt alloy on Pt(111) in Ag^+ free solution at ambient conditions is enabled by the strong interaction of the adsorbed cyanide with Ag and/or Pt, which possibly increases their surface mobility enabling their intermixing. We recently reported [23] that the reduction of Pd^{2+} preadsorbed on cyanide-modified Pt(111) also results in the direct deposition of Pd onto the Pt substrate, but no alloy formation was detected in that case, which is interesting considering the similitude between the lattice parameters of Pd and Pt (3.86 and 3.92 Å respectively) and the relatively larger difference in the case of Ag and Pt (4.08 and 3.92 Å respectively).

References

[1] H. Hagenström, M.A. Schneeweiss, D.M. Kolb, Copper underpotential deposition on ethanethiol-modified Au(111) electrodes: kinetic effects, Electrochim. Acta. 45 (1999) 1141–1145. https://doi.org/http://dx.doi.org/10.1016/S0013-4686(99)00314-X.

[2] M. Nishizawa, T. Sunagawa, H. Yoneyama, Underpotential Deposition of Copper on Gold Electrodes through Self-Assembled Monolayers of Propanethiol, Langmuir 13 (1997). https://doi:10.1021/la970545f

[3] O. Cavalleri, A.M. Bittner, H. Kind, K. Kern, Copper Electrodeposition on Alkanethiolate Covered

Gold Electrodes, Zeitschrift Phys. Chemie. 208 (1999) 107–136. https://doi.org/doi:10.1524/zpch.1999.208.Part_1_2.107.

[4] S.E. Gilbert, O. Cavalleri, K. Kern, Electrodeposition of Cu Nanoparticles on Decanethiol-Covered Au(111) Surfaces: An in Situ STM Investigation, J. Phys. Chem. 100 (1996) 12123–12130. doi:10.1021/jp960053w.

[5] M.A. Schneeweiss, H. Hagenström, M.J. Esplandiu, D.M. Kolb, Electrolytic metal deposition onto chemically modified electrodes, Appl. Phys. A. 69 (1999) 537–551. doi:10.1007/s003390051465.

[6] D. Oyamatsu, S. Kuwabata, H. Yoneyama, Underpotential deposition behavior of metals onto gold electrodes coated with self-assembled monolayers of alkanethiols, J. Electroanal. Chem. 473 (1999) 59–67. doi:10.1016/S0022-0728(99)00104-7.

[7] T. Baunach, V. Ivanova, D.M. Kolb, H.G. Boyen, P. Ziemann, M. Büttner, P. Oelhafen, A New Approach to the Electrochemical Metallization of Organic Monolayers: Palladium Deposition onto a 4,4'-Dithiodipyridine Self-Assembled Monolayer, Adv. Mater. 16 (2004) 2024–2028. doi:10.1002/adma.200400409.

[8] O. Shekhah, C. Busse, A. Bashir, F. Turcu, X. Yin, P. Cyganik, A. Birkner, W. Schuhmann, C. Woll, Electrochemically deposited Pd islands on an organic surface: the presence of Coulomb blockade in STM I(V) curves at room temperature, Phys. Chem. Chem. Phys. 8 (2006) 3375–3378. doi:10.1039/B606488D.

[9] C. Silien, D. Lahaye, M. Caffio, R. Schaub, N.R. Champness, M. Buck, Electrodeposition of Palladium onto a Pyridine-Terminated Self-Assembled Monolayer, Langmuir. 27 (2011) 2567–2574. doi:10.1021/la104561j.

[10] M.I. Muglali, J. Liu, A. Bashir, D. Borissov, M. Xu, Y. Wang, C. Wöll, M. Rohwerder, On the complexation kinetics for metallization of organic layers: palladium onto a pyridine-terminated araliphatic thiol film, Phys. Chem. Chem. Phys. 14 (2012) 4703–4712. doi:10.1039/c2cp40072c.

[11] D. Qu, K. Uosaki, Electrochemical Metal Deposition on Top of an Organic Monolayer, J. Phys. Chem. B. 110 (2006) 17570–17577. doi:10.1021/jp0632135.

[12] M. Manolova, V. Ivanova, D.M. Kolb, H.G. Boyen, P. Ziemann, M. Büttner, A. Romanyuk, P. Oelhafen, Metal deposition onto thiol-covered gold: Platinum on a 4-mercaptopyridine SAM, Surf. Sci. 590 (2005) 146–153. doi:10.1016/j.susc.2005.06.005.

[13] F. Eberle, M. Saitner, H.G. Boyen, J. Kucera, A. Gross, A. Romanyuk, P. Oelhafen, M. D'Olieslaeger, M. Manolova, D.M. Kolb, A molecular double decker: Extending the limits of current metal-molecule hybrid structures, Angew. Chemie Int. Ed. 49 (2010) 341–345. doi:10.1002/anie.200905339.

[14] J.A. Mwanda, A. Cuesta, Electrochemical metallization of molecular adlayers, Curr. Opin. Electrochem. 17 (2019) 72–78. doi:10.1016/j.coelec.2019.04.022.

[15] C.S. Kim, C. Korzeniewski, Cyanide adsorbed as a monolayer at the low-index surface planes of platinum metal electrodes: an in situ study by infrared spectroscopy, J. Phys. Chem. 97 (1993) 9784–9787. doi:10.1021/j100140a041.

[16] C. Stuhlmann, I. Villegas, M.J. Weaver, Scanning tunneling microscopy and infrared spectroscopy as combined in situ probes of electrochemical adlayer structure. Cyanide on Pt(111), Chem. Phys. Lett. 219 (1994) 319–324. doi:10.1016/0009-2614(94)87064-0.

[17] V.B. Paulissen, C. Korzeniewski, Infrared spectroscopy as a probe of the adsorption and electrooxidation of a cyanide monolayer at platinum under aqueous electrochemical conditions, J. Phys. Chem. 96 (1992) 4563–4567. doi:10.1021/j100190a079.

[18] M. Escudero-Escribano, G.J. Soldano, P. Quaino, M.E. Zoloff Michoff, E.P.M. Leiva, W. Schmickler,

Á. Cuesta, Cyanide-modified Pt(111): Structure, stability and hydrogen adsorption, Electrochim. Acta. 82 (2012) 524–533. doi:10.1016/j.electacta.2012.02.062.

[19] M. Escudero, A. Cuesta, Electrocatalysis and Surface Nanostructuring : Atomic Ensemble Effects and Non-Covalent Interactions, Universidad Autónoma de Madrid, 2011. http://hdl.handle.net/10261/42378.

[20] M. Escudero-Escribano, M.E. Zoloff Michoff, E.P.M. Leiva, N.M. Marković, C. Gutiérrez, A. Cuesta, Quantitative Study of Non-Covalent Interactions at the Electrode-Electrolyte Interface Using Cyanide-Modified Pt(111) Electrodes, ChemPhysChem. 12 (2011) 2230–2234. doi:10.1002/cphc.201100327.

[21] M. Escudero, J.F. Marco, A. Cuesta, Surface Decoration at the Atomic Scale Using a Molecular Pattern: Copper Adsorption on Cyanide-Modified Pt(111) Electrodes, J. Phys. Chem. C. 113 (2009) 12340–12344. doi:10.1021/jp901643q.

[22] M. Escudero-Escribano, C. Wildi, J.A. Mwanda, A. Cuesta, Metallization of cyanide-modified Pt(111) electrodes with copper, J. Solid State Electrochem. 20 (2016) 1087–1094. doi:10.1007/s10008-015-2968-7.

[23] J.A. Mwanda, A. Cuesta, Reduction of Pd^{2+} pre-adsorbed on cyanide-modified Pt(111) electrodes: Adlayer metallization vs. metal-on-metal deposition, Electrochim. Acta. 292 (2018) 419–424. doi:10.1016/j.electacta.2018.08.120.

[24] J. Clavilier, R. Faure, G. Guinet, R. Durand, Preparation of monocrystalline Pt microelectrodes and electrochemical study of the plane surfaces cut in the direction of the {111} and {110} planes, J. Electroanal. Chem. 107 (1979) 205–209. doi:10.1016/S0022-0728(79)80022-4.

[25] C. Wildi, G. Cabello, M.E. Zoloff Michoff, P. Velez, E.P.M. Leiva, J.J. Calvente, R. Andreu, A. Cuesta, Super-Nernstian Shifts of Interfacial Proton-Coupled Electron Transfers: Origin and Effect of Noncovalent Interactions, J. Phys. Chem. C. 120 (2016) 15586–15592. doi:10.1021/acs.jpcc.5b04560.

[26] F. Huerta, E. Morallón, J. Vázquez, Voltammetric analysis of the co-adsorption of cyanide and carbon monoxide on a Pt(111) surface, Electrochem. Commun. 4 (2002) 251–254. doi:10.1016/S1388-2481(02)00271-0.

[27] I. Morales-Moreno, A. Cuesta, C. Gutierrez, Accurate determination of the CO coverage at saturation on a cyanide-modified Pt(111) electrode in cyanide-free 0.5 M H2SO4, J. Electroanal. Chem. 560 (2003) 135–141. doi:10.1016/j.jelechem.2003.07.008.

[28] S. Beckord, A.K. Engstfeld, S. Brimaud, R.J. Behm, Electrochemical Characterization and Stability of Ag_xPt_{1-x}/Pt(111) Surface Alloys, J. Phys. Chem. C. 120 (2016) 16179–16190. doi:10.1021/acs.jpcc.6b00528.

[29] S. Beckord, S. Brimaud, R.J. Behm, Stability and ORR performance of a well-defined bimetallic $Ag_{70}Pt_{30}$/Pt(111) monolayer surface alloy electrode – Probing the de-alloying at an atomic scale, Electrochim. Acta. 259 (2018) 762–771. doi:10.1016/J.ELECTACTA.2017.10.146.

[30] F. Huerta, F. Montilla, E. Morallón, J.L. Vázquez, On the vibrational behaviour of cyanide adsorbed at Pt(111) and Pt(100) surfaces in alkaline solutions, Surf. Sci. 600 (2006) 1221–1226. doi:10.1016/j.susc.2005.12.046.

[31] F. Huerta, E. Morallón, J.L. Vázquez, Structural effects of adsorbed CN adlayers on the co-adsorption of OH− at the Pt(111) surface in sulfuric acid medium, Surf. Sci. 431 (1999) L577–L581. https://doi.org /10.1016/S0039-6028(99)00580-4.

[32] Y.-G. Kim, S.-L. Yau, K. Itaya, Direct Observation of Complexation of Alkali Cations on Cyanide-Modified Pt(111) by Scanning Tunneling Microscopy, J. Am. Chem. Soc. 118 (1996) 393–400.

doi:10.1021/ja9521841.

[33] A.K. Engstfeld, H.E. Hoster, R.J. Behm, Formation, atomic distribution and mixing energy in two-dimensional Pd_xAg_{1-x} surface alloys on Pd(111), Phys. Chem. Chem. Phys. 14 (2012) 10754. doi:10.1039/c2cp41104k.

[34] H.E. Hoster, A. Bergbreiter, P.M. Erne, T. Hager, H. Rauscher, R.J. Behm, Pt_xRu_{1-x}/Ru(0001) surface alloys—formation and atom distribution, Phys. Chem. Chem. Phys. 10 (2008) 3812. doi:10.1039/b802169d.

[35] P. Ocón, P. Herrasti, C. Palacio, M.E. Vela, R.C. Salvarezza, L. Vazquez, A. Arvia, The role of slow surface-atom reordering processes in the underpotential deposition of metals Silver underpotential deposition on platinum in acid solutions, J. Electroanal. Chem. 357 (1993) 339–355. https:// doi:10.1016/0022-0728(93)80390-4

[36] H. Röder, R. Schuster, H. Brune, K. Kern, Monolayer-Confined Mixing at the Ag-Pt(111) Interface, Phys. Rev. Lett. 71 (1993) 2086–2091. https:// doi:10.1103/PhysRevLett.71.2086

[37] H. Röder, H. Brune, J.-P. Bucher, K. Kern, Changing morphology of metallic monolayers via temperature controlled heteroepitaxial growth, Surf. Sci. 298 (1993) 121–126. doi:10.1016/0039-6028(93)90088-2.

We would be delighted to provide a Credit Author Statement, if you were just so nice to explain what this is and what information is required in that statement. The help available in your Editorial Manager is not helpful at all in this regard.

Declaration of Interest

The authors declare no conflict of interest.

Reduction of Ag^+ irreversibly adsorbed on cyanide-modified Pt(111)

Jonathan A. Mwanda†, Angel Cuesta*

Department of Chemistry, School of Natural and Computing Sciences, University of Aberdeen, AB24 3UE, Scotland, UK

†Current address: Gulf Organization for Research and Development, Doha, Qatar

*Corresponding author: angel.cuestaciscar@abdn.ac.uk

ABSTRACT

We report a study of the electrochemical reduction of Ag^+ immobilized on a cyanide modified Pt(111) electrode in a Ag^+-free solution using cyclic voltammetry and in-situ STM. We show that, upon reduction at 0.29 V, Ag deposits directly on the platinum substrate, resulting in the formation of an AgPt surface alloy without loss of the cyanide adlayer The large affinity of Ag^+ for CN_{ad} is responsible for this large negative shift of the Ag^+/Ag redox couple.. A fraction of the electrodeposited Ag is reoxidised at 0.34 V to yield again Ag^+ coordinated to the CN adlayer. Therefore, successive cycling with a positive limit below 0.90 V results in a roughening of the surface and in the gradual transformation of cyanide-modified Pt(111) to a cyanide-modified AgPt surface alloy on Pt(111).

Keywords: Cyclic voltammetry; STM; electroreduction; Metallization; cyanide-modified Pt(111); Surface alloy

5 Introduction

Initial attempts to metallize molecular adlayers electrochemically (a particularly attractive method due to the low cost and simplicity of the equipment required) failed [1–6], with the deposited metal effectively creeping underneath and depositing on the metal substrate. In 2004 however, Kolb et al. [7] demonstrated the successful electrochemical metallization of a molecular adlayer via the immobilization of a metal cation on a self-assembled monolayer (SAM) of an adequately functionalised molecule, followed by reduction in a metal free solution. Various groups have since demonstrated the metallization of SAMs employing electrochemical reduction techniques [8–11], although yielding 3D islands instead of the 2D islands reported by Kolb et al. [7,12,13]. For a recent review on this subject see [14].

The metallization of a SAM with an ordered array of metal islands of the same size would lead to a high density of molecular contacts per unit area, all with the same number of molecules sandwiched between the bidimensional metal island and the metallic substrate. In addition to the high density of circuit elements per unit area, such ordered array could have interesting properties associated to plasmon excitations or collective phenomena. Achieving this goal would require a nanopatterned SAM with an ordered distribution of equivalent adsorption sites, and a way to limit the diffusion of pre-adsorbed metal ions, thus limiting the aggregation and migration over the SAM of the bidimensional metal islands during and after the reduction step. We have attempted to reach this goal (unfortunately without success until now) by metallizing cyanide-modified Pt(111) electrodes using Kolb's method.

Cyanide adsorbs spontaneously and irreversibly on Pt(111), with the carbon end bonded linearly on-top of a platinum atom and the nitrogen end pointing into the solution, forming a (2√3 x 2√3) *R*30° structure [15–17]. We have shown that alkaline-metal cations [18–20], Cu^{2+} [19,21,22] and Pd^{2+} [23] adsorb on the cyanide adlayer due to the electrostatic interaction of the cation with the negative end of the dipole of adsorbed cyanide, this adsorption being irreversible in the case of Cu^{2+} [19,21,22] and Pd^{2+} [23]. In-situ STM images of cyanide-modified Pt(111) electrodes in solutions containing Na^+, K^+, Cs^+ or Cu^{2+}, as well as of cyanide-modified Pt(111) electrodes with pre-adsorbed Cu^{2+} or Pd^{2+} in solutions free of the corresponding cation, show in all cases the formation of a honeycomb pattern, suggesting the adsorption of the cations around the CN rings at sites in which the cation interacts with the N atom of three CN groups [18,20–23].

Attempts to reduce the immobilised Cu^{2+} in Cu^{2+}-containing solutions failed to metallize the adlayer, resulting in the direct deposition of Cu onto the Pt substrate [21]. However, bidimensional Cu nanoislands were formed on the cyanide adlayer when Kolb's method was employed [22]. These islands were shown to deposit and dissolve reversibly, and to grow via an Ostwald's ripening process. Differences observed attempting to metallize the cyanide with Cu [22] and Pd [23] suggest that the interaction of the metal with the SAM might play an important role in determining the result of the electrodeposition process. In this work, we report on the attempt to metallize the cyanide adlayer on cyanide-modified Pt(111) electrodes by reducing Ag^+ ions immobilised on the cyanide SAM in Ag^+-free sulphuric acid solutions.

6 Experimental

The working electrode used for cyclic voltammetry (CV) was a bead type platinum single crystal (2 mm diameter) prepared according to the method developed by Clavilier et al. [24], oriented and polished

parallel to the (111) plane (miscut < 0.05°). For electrochemical scanning tunnelling microscopy (EC-STM) experiments, the Pt(111) electrode used was a single-crystal disc (10 mm in diameter) purchased from MaTeck (Jülich, Germany, miscut < 1^{o}). Before every experiment, the electrodes were flame annealed in a Bunsen burner and cooled in a H_2/N_2 reductive atmosphere. Once cold, a drop of Milli-Q water (18 MΩ cm, 2 ppb TOC) saturated with the cooling N_2 and H_2 mixture was attached to the exposed (111) surface in order to protect it during transport through the laboratory's atmosphere.

Cyanide-modified Pt(111) electrodes were prepared by immersing, immediately after the step described above, a clean and well-ordered Pt(111) electrode in a 0.1 M KCN (Merck, pa) solution for approximately 3 min, after which the electrode was rinsed with ultrapure water. Pre-adsorption of Ag^+ was achieved by immersing the cyanide-modified Pt(111) electrode in 0.1 M $HClO_4$ + 1 mM $AgClO_4$ for approximately 3 min, followed by rinsing with Milli-Q water. All the experiments were carried out in Ag^+-free 0.1 M H_2SO_4. Solutions were prepared from concentrated H_2SO_4 (Merck, Suprapur) and $AgClO_4 \cdot H_2O$ (Sigma Aldrich, 99.99% trace metal analysis). All CVs were measured after degassing the solution with N_2 (BOC, Research Grade N5.5).

Platinum wires (Alfa Aesar 99.997%, 0.5 mm in diameter) were utilized as auxiliary electrodes. A reversible hydrogen electrode (RHE) and a Pt wire were used as reference and quasi-reference electrode, respectively, for CV and EC-STM, respectively. All potentials in the text are referred to the RHE scale, unless otherwise stated.

STM images were recorded using a PicoLe Molecular Imaging with a PicoScan 2100 controller. Tungsten tips for STM experiments were etched from a polycrystalline W wire (0.25 mm in diameter) in 2 M NaOH and coated with electrophoretic paint to minimize the faradaic current at the tip/electrolyte interface. All images were acquired in the constant-current mode.

7 Results and Discussion

7.1 Cyclic Voltammetry

Cyanide-modified Pt(111) electrodes with pre-adsorbed Ag^+ were immersed in Ag^+-free 0.1 M H_2SO_4 at 0.80 V, and a CV at 0.05 V s^{-1} was then started with a potential sweep in the negative direction. The first and second CVs are shown in Fig. 1, solid and dotted black lines respectively. The CV of the same electrode if, after immersion in the same electrolyte, cycling is kept within the potential region between 0.6 and 1.10 V, as well as that of a cyanide-modified Pt(111) in 0.1 M H_2SO_4 without pre-adsorbed Ag^+ (red line), are also shown for comparison.

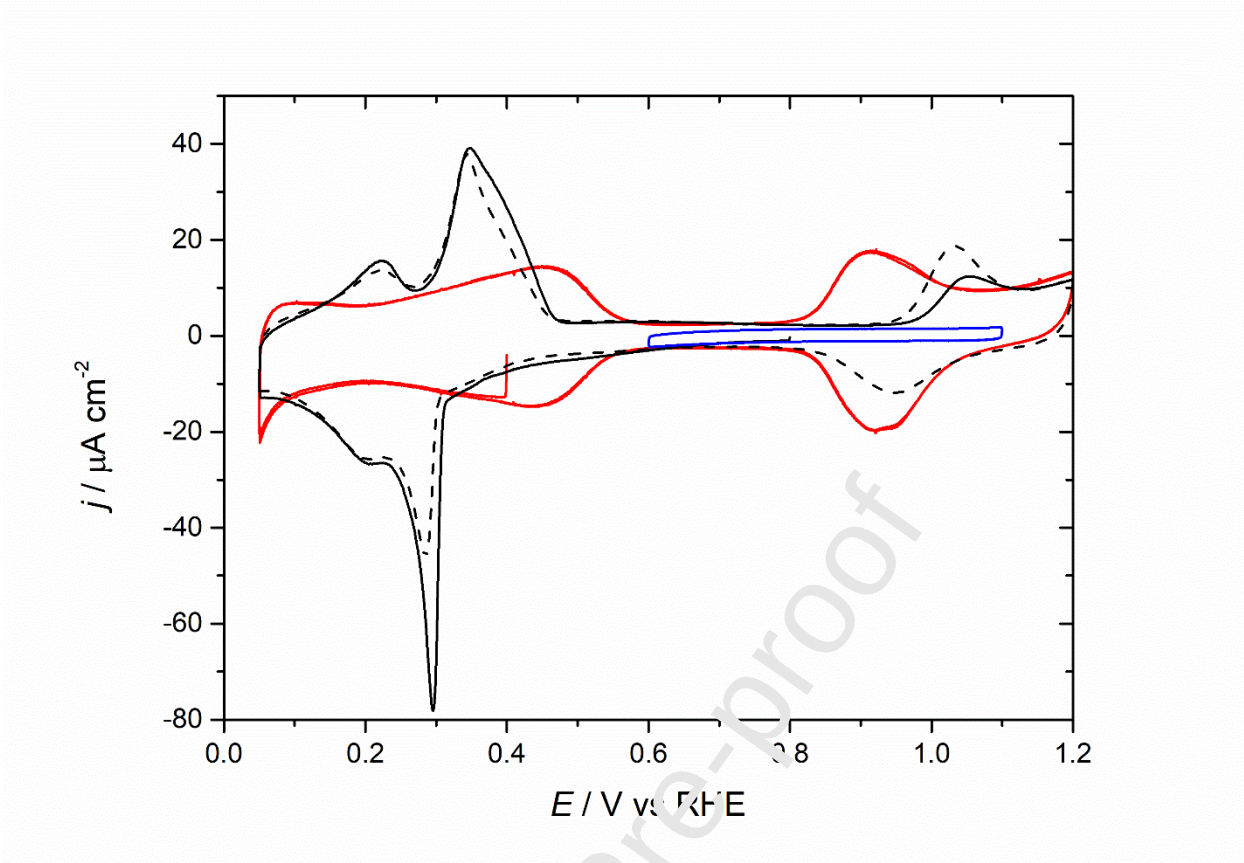

Figure 4. First (solid black line) and second (dotted line) cyclic voltammograms in Ag^+-free 0.1 M H_2SO_4 of a cyanide-modified Pt(111) electrode on which Ag^+ had been pre-adsorbed. The blue line corresponds to the cyclic voltammogram of the same electrode in the same solution if the negative potential limit is kept above 0.6 V, thereby preventing the reduction of pre-adsorbed Ag^+. The red line corresponds to the cyclic voltammogram of a cyanide-modified Pt(111) electrode without pre-adsorbed Ag^+ in the same electrolyte. Scan rate: 0.05 V s^{-1}.

The CV of cyanide-modified Pt(111) (red line) is characterized by a broad reversible feature between 0.05 and 0.50 V, corresponding to a proton-electron transfer to CN_{ad} to form $(CN)_xH_{ad}$, with x decreasing with increasingly negative potential [18]. We have previously demonstrated that M^{z+} cations can interact electrostatically with the negative partial charge on the nitrogen atom of CN_{ad}, and that, depending on the cation, this can result either in the reversible adsorption of the cation on the cyanide-modified Pt(111) surface [20,21], or in irreversible adsorption [22,23]. In all cases, adsorption of M^{z+} on cyanide-modified Pt(111) results in a negative shift of the onset of hydrogen adsorption, due to the competition between M^{z+} and H^+ for the same adsorption sites on the cyanide adlayer. This is also observed in Fig. 1, providing evidence of the irreversible complexation of Ag^+ with CN_{ad}.

A second surface process appears just above 0.90 V in the CV of cyanide-modified Pt(111) which, although still not clearly identified, have been associated with the adsorption of oxygenated species such as OH [26,27]. In the presence of pre-adsorbed Ag^+, this process is completely blocked as long as the negative potential limit is kept more positive than 0.60 V (Figure 1, blue line), thereby preventing the reduction of pre-adsorbed Ag^+. This suggests either that (i) the adsorption process around 0.90 V involves the nitrogen atoms of the CN_{ad} groups, which are blocked by pre-adsorbed Ag^+ or (ii) pre-adsorbed Ag^+ ions prevent the access of water molecules to the surface of the Pt(111), inhibiting the formation of OH_{ad} on Pt.

If the negative potential limit is extended below 0.60 V, a new reduction peak emerges in the first negative sweep at 0.29 V (Figure 1, black solid line). The corresponding anodic counterpart appears as an asymmetric peak at 0.34 V. It is reasonable to attribute the cathodic peak at 0.29 V to the reduction of Ag^+ coordinated to CN_{ad} to Ag, and the peak at 0.34 V to the reverse process:

$$\mathrm{CN_{ad}} - \mathrm{Ag^+} + \mathrm{e^-} \rightleftharpoons \mathrm{Ag} + \mathrm{CN_{ad}} \quad (1)$$

Please note that this is much more negative than the standard equilibrium potential for the Ag^+/Ag couple (0.86 V *vs.* RHE at this pH), therefore, the anodic peak at 0.34 V cannot correspond to the oxidation of Ag to aqueous Ag^+. However, oxidation of Ag at this potential is still possible if the final state is Ag^+ coordinated to CN_{ad} due to the strong interaction of Ag^+ with CN_{ad} (otherwise adsorption of Ag^+ on cyanide-modified Pt(111) would not be irreversible). This results in a considerable stabilization of the oxidised form of this couple (CN_{ad}–Ag^+) which contributes to the significant negative shift of the corresponding equilibrium potential. The same peak, albeit less intense, appears in the second negative sweep (Figure 1, dotted black line). The difference between the charge density in the first and second negative sweeps amounts to ca. 17.0 μC cm^{-2}, suggesting that less CN_{ad}-attached Ag^+ is available for reduction to Ag in the second sweep. We will discuss this in more depth below.

A reversible process around 0.20 V appears immediately after the negative peak at 0.29 V. A similar reversible peak has been observed in the voltammetric profile of $AgPt_{1-x}$/Pt(111) surface alloys, and has been attributed to the adsorption of hydrogen on alloys with a Ag content higher than 50% [28,29]. This suggests that reduction of CN_{ad}-coordinated Ag^+ at 0.29 V results in the immediate formation of a surface AgPt alloy with a local content of Ag higher than 50%, and that the silver slowly disperses throughout the Pt(111) surface upon repeated cycling.

Following the reduction processes described above, the surface process observed around 0.90 V in the CV of cyanide-modified Pt(111) (see Fig. 1, red line) re-emerges after the first negative potential excursion, but now at a slightly more positive potential around 1.0 V. This peak at ca. 1.0 V appears less symmetrical and slightly more positive than the peaks around 0.9 V on cyanide-modified Pt(111) (see Fig. 1, red line). It is reasonable to also ascribe the new process to the adsorption of oxygenated species such as OH, as the peaks occurring around 0.9 V on the cyanide modified Pt(111) [26,27]. The positive shift and differing shape of the peaks is possibly due to OH adsorption on a cyanide-modified AgPt alloy, as opposed to cyanide-modified on Pt(111).

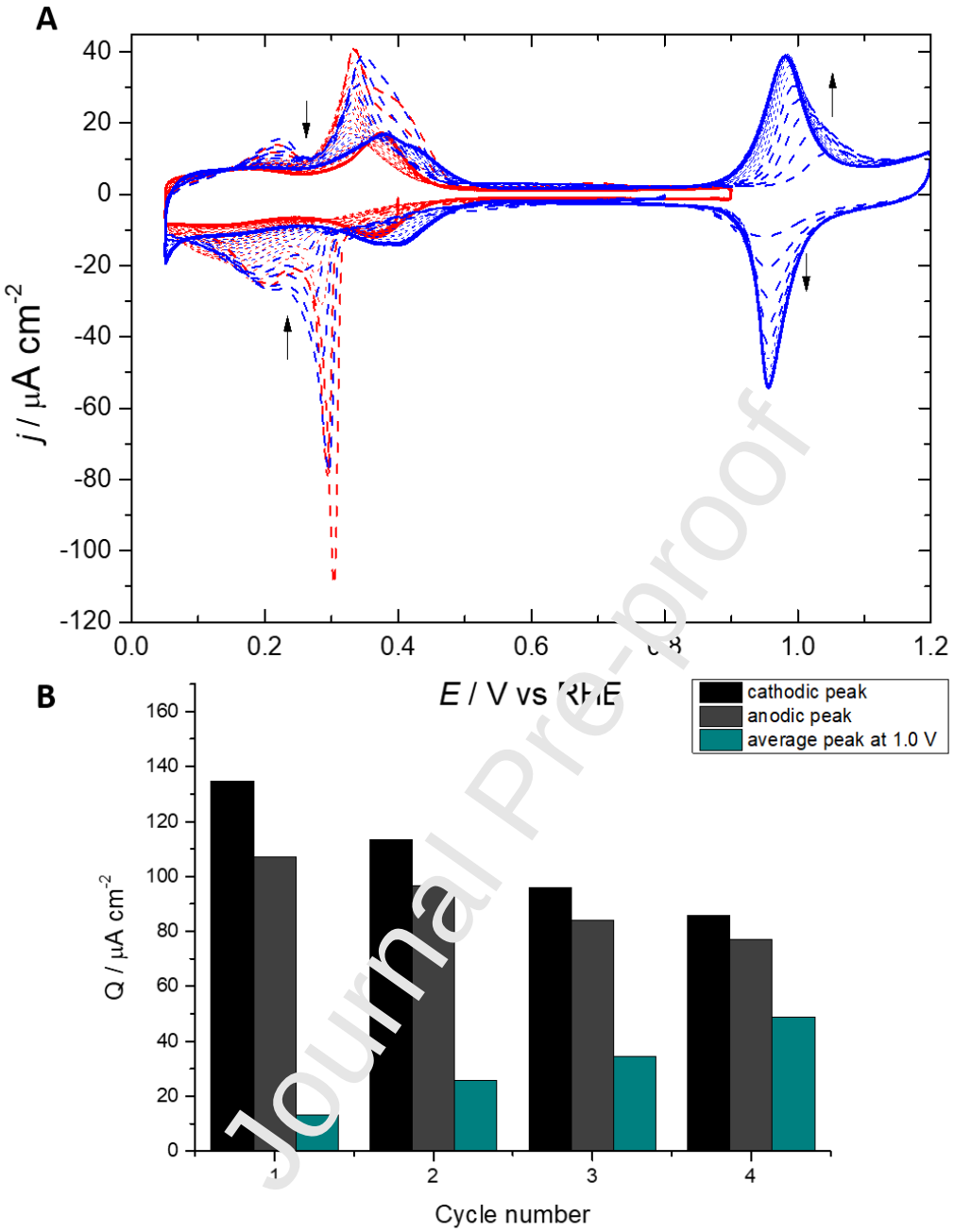

Figure 5. A: Evolution of the cyclic voltammogram in 0.1 M H_2SO_4 of a cyanide-modified Pt(111) electrode on which Ag^+ had been pre-adsorbed with successive cycling between 0.05 and 1.20 V (blue line) and between 0.05 and 0.9 V (red line) at a scan rate of 0.05 V s^{-1}. The blue and red solid lines indicate the final steady state, and the black arrows indicate the direction of evolution of the voltammetric profile. **B:** Bar graph showing the charge density obtained by integration of the CV between 0.1 and 0.5 V in the negative (black) and positive (grey) potential sweeps of the first four cycles. The horizontal red dashed lines highlight the clear correlation between the charge density in the cathodic sweep and that in the subsequent anodic sweep.

Fig. 2 A illustrates the evolution with successive cycling of the CV in 0.1 M H_2SO_4 of a cyanide-modified Pt(111) electrode on which Ag^+ had been pre-adsorbed. The first negative scan when the positive potential limit is set to 1.2 V (blue lines), overlaps with the first negative scan when the positive limit is 0.9 V (red lines) and therefore has not been included in the figure. Independently of the positive

potential limit, upon successive cycling the peaks at 0.29 (cathodic) and 0.34 (anodic) V attributed to the $Ag^+(CN_{ad})/Ag$ couple decrease in intensity. Similarly, the reversible process around 0.20 V, attributed to the adsorption of hydrogen on a surface AgPt alloy with a Ag local content higher than 50% continuously decreases in intensity, until its practical disappearance. Regarding the process around 1.0 V (obviously only observable when the potential limit is increased from 0.9 to 1.2 V), attributed to the adsorption of oxygenated species on the cyanide modified AgPt alloy, it becomes more reversible and increases in intensity with repeated cycling, mirroring the decrease in intensity of the processes at 0.29/0.34 V and around 0.20 V. The decrease of the charge density associated with the latter processes is illustrated in the bar chart in Fig. 2 B, which shows the double-layer corrected charge densities in the potential region between 0.1 and 0.5 V for the first four cycles. Double layer correction was done by assuming that the double-layer capacitance, as estimated from the current between 0.6 and 0.8 V, remains constant over the whole voltammetric potential range, and subtracting the charge density corresponding to that capacitance between 0.1 and 0.5 V from that resulting from integrating the CV within that potential region. (Please note that the current and the charge density in this region mainly corresponds to hydrogen adsorption on the cyanide adlayer and, upon eventual partial stripping of CNad, of Pt and PtAg alloy regions. The charge corresponding to silver deposition is relatively small and concentrated within the peak at approximately 0.30 V.)

The continuous decrease of the overall charge density in this potential region suggests a continuous decrease in the amount of pre-adsorbed Ag^+ ions coordinated to CN_{ad} available for reduction. Of interest is the good match between the anodic charge density in a given cycle and the cathodic charge density in the subsequent cycle, as highlighted by the red dashed lines in Fig. 2 B. This suggests that the amount of Ag^+ reduced in cycle $n + 1$ corresponds to the fraction of Ag^+ produced by oxidation of Ag in the surface AgPt alloy in cycle n that had re-adsorbed on the CN_{ad}, thus confirming our assignment of the process at 0.29/0.34V to the $Ag^+(CN_{ad})/Ag$ redox couple.

The reduction in the charge density associated to the redox process at 0.29/0.34 V is accompanied by a decrease in the reversible peaks occurring at ca. 0.20 V (Fig. 2 A). This decrease suggests that, although the total amount of Ag in the AgPt surface alloy increases with cycling, the dilution of Ag in the alloy also increases. This apparent contradiction can be explained by considering that the presence of the reversible process at 0.20 V characteristic of $Ag_xPt_{1-x}/Pt(111)$ surface alloys with more than 50% will be determined by the local concentration of Ag. Initially, the alloy forms only on those regions where silver penetrates the cyanide adlayer and, although the total amount of Ag deposited is small, it results in a high local concentration above 50%. The maximum amount of Ag^+ that can be adsorbed on CN_{ad} in the honeycomb structure amounts to 0.16 ML [18,20,22,23] thus the overall concentration of Ag in the alloy can never approach 50%. During cycling, the mobility of Ag within the surface decreases the inhomogeneity in the local Ag concentration and the local Ag concentration of the surface alloy slowly approaches the overall Ag concentration, with a limiting value of 0.16 ML, thus explaining the continuous decrease in the reversible peaks around 0.20 V.

From previous work by our group [27] and others [30], we know that oxidative stripping of adsorbed cyanide starts above 1.1 V. The differences between the final, steady state voltammogram, when positive scan limits of either 0.90 V (Fig. 2A, red-dashed lines) or 1.2 V (Fig. 2 A blue-dashed lines) are used can be attributed, therefore, to the disruption of the cyanide layer above 1.1 V. The main difference is observed in the region between 0.05 and 0.5 V, in which the charge density is 17.2 $\mu C\ cm^{-2}$ for the more positive potential limit. As shown by Huerta et al. [31], this extra charge must correspond to sulphate adsorption within the cyanide-free Pt(111) patches left free upon partial stripping of the cyanide adlayer.

The evolution of the peaks just below 1 V with successive cycling is the result from several contributions. Although PtAg surface alloys do not show any voltammetric peak in this region [28] (and therefore, these peaks cannot be attributed to the oxidation-reduction of the PtAg surface), dissolution of Ag from the surface alloy has been demonstrated to start around 0.95 V [29] and must contribute to this current, particularly in the first cycles. This is confirmed by the roughening of the electrode surface in this potential region as revealed by in-situ STM (see below). Peaks in this potential region are also absent on a naked Pt(111) surface, but emerge upon cyanide adsorption and increase in intensity with increasing cyanide coverage [31]. However, even for the highest possible cyanide coverage the peaks are not as sharp as in Fig. 2A (see, e.g., the CV of cyanide-modified Pt(111) in Fig. 1, red line). Based on these arguments, we assign the reversible peaks around 1 V in the CV in Fig. 2A to the adsorption of OH on a rough PtAg surface alloy on Pt(111) covered by a perturbed cyanide adlayer. In the case of the CV with a positive scan limit of 1.2 V (blue line in Fig. 2A), the Ag content of the surface alloy and the cyanide coverage must be lower than when the potential limit is kept below 0.9 V, due to partial dissolution of Ag and partial stripping of the cyanide adlayer, respectively.

7.2 EC-STM

EC-STM was used to monitor the surface structure and morphology changes associated to the voltammetric features as described in the previous section.

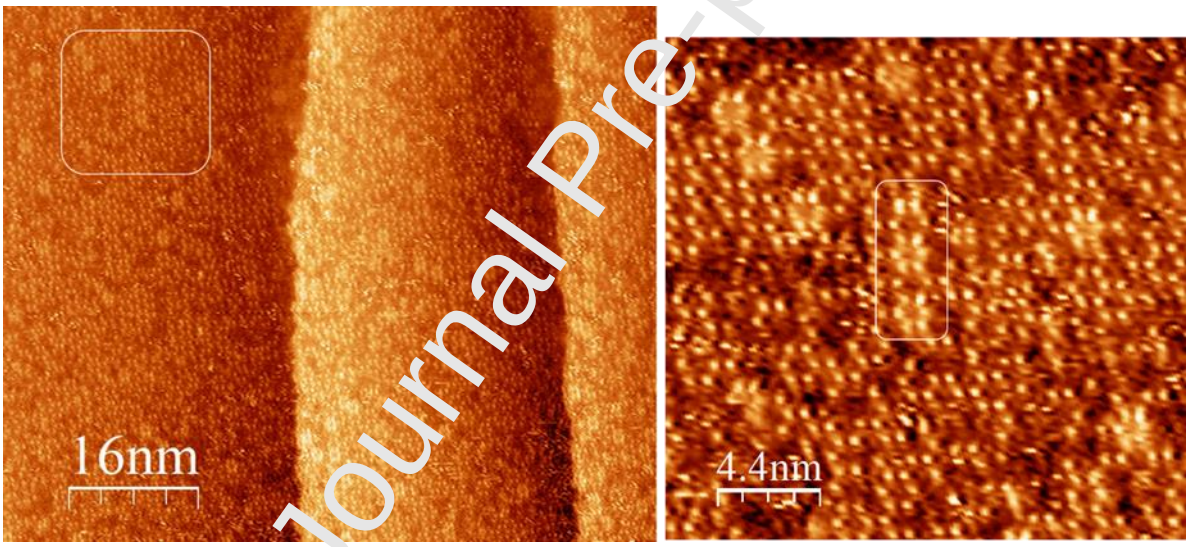

Figure 6. In-Situ STM images of a cyanide-modified Pt(111) on which Ag^+ had been pre-adsorbed in Ag^+-free 0.1 M H_2SO_4 at E= 0.80 V, U_T = 0.50 V (tip negative); I_T = 2 nA. The image in the left panel corresponds to an area 80 x 69 nm^2, while the right panel is a zoom in corresponding to the white square in the left panel (22 x 21 nm^2).

Fig. 3 shows STM images in Ag^+-free 0.1 M H_2SO_4 at 0.80 V of a cyanide modified Pt(111) electrode on which Ag^+ had been pre-adsorbed. Tunnelling maxima forming a honeycomb pattern cover the whole surface, but for some defects within the structure. Similar honeycomb structures have been observed by EC-STM upon irreversible adsorption of Cu^{2+} [22] on cyanide-modified Pt(111) electrodes, as well as on cyanide-modified Pt(111) electrodes immersed in acidic solutions containing Li^+, Na^+, K^+ or Cs^+ above a cation-specific threshold concentration [20]. A typical STM image of a cyanide modified Pt(111) without pre-adsorbed cations or in solutions containing Li^+, Na^+, K^+ or Cs^+ below their corresponding threshold concentration can be found in the supporting information to reference [20], and is identical to those reported decades ago by other groups for the (2√3 x 2√3) R30° structure of cyanide on Pt(111)

[16,32]. The honeycomb pattern observed in Fig. 3 is therefore also attributed in this case to non-covalently coordinated Ag^+ on the cyanide SAM.

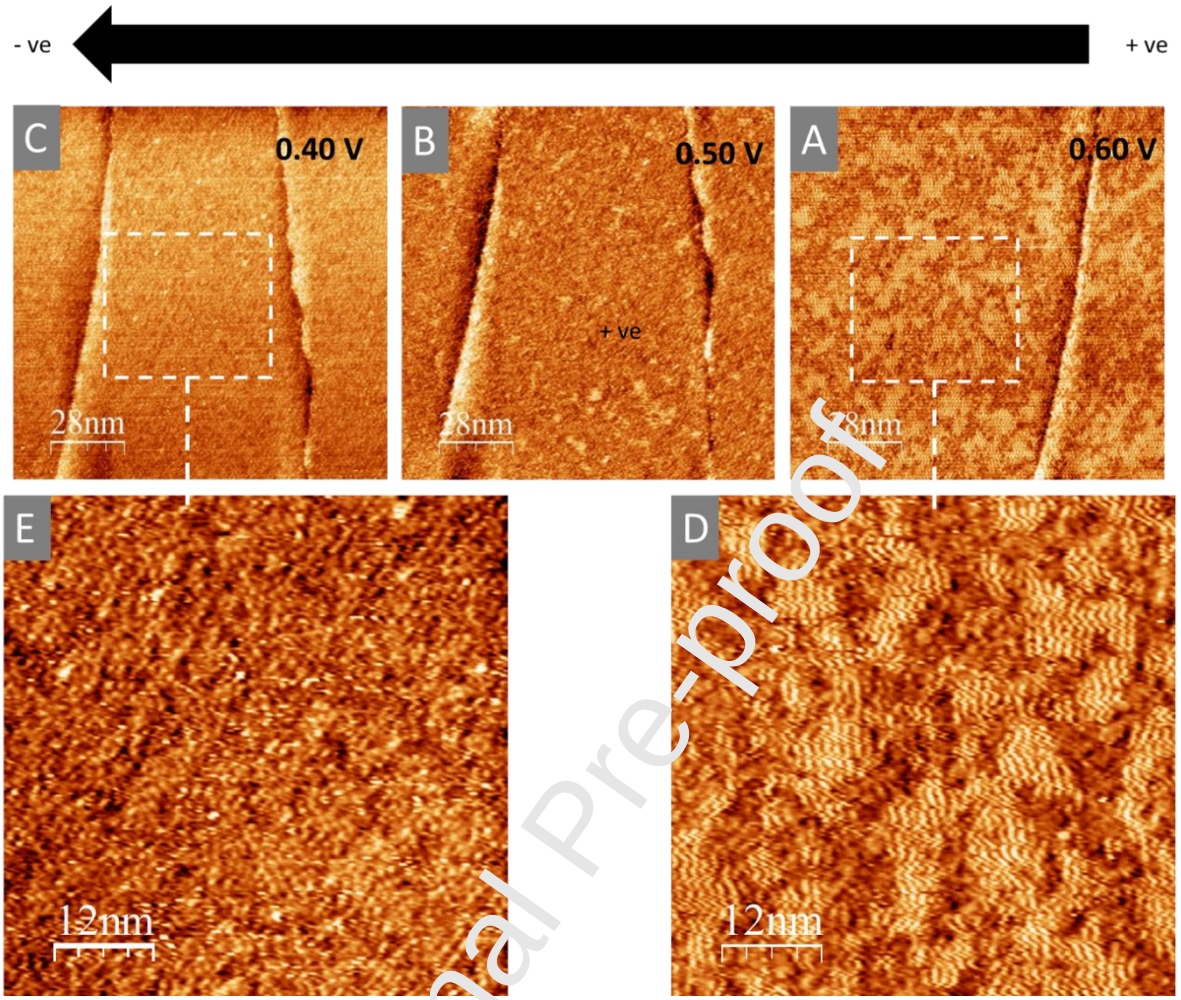

Figure 4. In-situ STM images (140 x 140 nm^2) recorded during the reduction of Ag^+ pre-adsorbed on a cyanide modified Pt(111) electrode in Ag^+-free 0.1 M H_2SO_4. Images recorded during the sequential reduction of the pre-adsorbed Ag^+, from left to right **(A)** E = 0.60 V, U_T = 0.40 V, **(B)** E = 0.50 V, U_T = 0.30 V, **(C)** E = 0.40 V, U_T = 0.20 V. Images (**D**) and (**E**) are 60 x 60 nm^2 zoom-ins corresponding to the dashed white squares in images **A** and **B**, respectively. All images acquired with tip negative biases and at I_T = 2 nA.

Figs. 4 A, B and C correspond to a series of STM images acquired sequentially from positive to more negative potentials (direction of black arrow) at 0.60, 0.50 and 0.40 V. At 0.60 V, the areas covered by the honeycomb structure observed at 0.80 V transform into high contrast areas containing zig zag lines running parallel to each other and separated by ca. 1 nm. This slight change is not accompanied by any voltammetric feature, which is most likely due to the slow rate of this process and the different time scales of the voltammetric and the STM experiments. As shown clearly in Fig. 4 D, the zigzag lines tend to align in three rotational domains rotated ca. 120° with respect to each other. The periodicity of the lines and the three rotational domains aligned with the substrate's main crystallographic directions suggest they correspond to edges of the hexagons formed by Ag^+ cations in the honeycomb structure on cyanide-modified Pt(111). The observation of edges rather than individual spots, like at 0.80 V, is attributed to an increased mobility leading to Ag^+ ions moving more easily among adsorption sites. In this scenario, the orientation of the line would indicate the direction along which the cations are moving when transiting among adsorption sites, thus explaining why only some of the edges of the hexagons

constituting the honeycomb can be observed. The reason behind the increased mobility of the Ag^+ ions in the honeycomb at this potentials and not more positive potentials is possibly connected to ion pairing with (bi)sulphate ions from the electrolyte, as discussed below.

A potential step from 0.60 to 0.50 V is accompanied by the vanishing of ca. 80% of the high contrast areas, which disappear completely (but reversibly if the potential is not stepped into the Ag deposition region) at 0.40 V. It is not very clear what is provoking this disappearance, as there is no feature in the CV in this potential region (see Fig. 1), but preliminary simulations of STM images using DFT suggest that, with the tunnelling biases employed, the density of states (DOS) of unoccupied energy levels on the cations coordinated to the cyanide adlayer at energies below the tip's Fermi level (allowing for tunnelling from the negatively biased tip to the cations) is zero and they should not be visible to STM, unless forming ionic pairs with oxyanions like sulphate or perchlorate, which leads to the emergence of empty DOS. Therefore, we provisionally attribute the apparent vanishing of the honeycomb features to the release of sulphate from these ionic pairs as the negative charge density on the Pt(111) substrate increases (at potentials more negative). We also suggest that partial release of sulphate in these ionic pairs is responsible for the increased mobility observed at 0.60 V and discussed in the paragraph above.

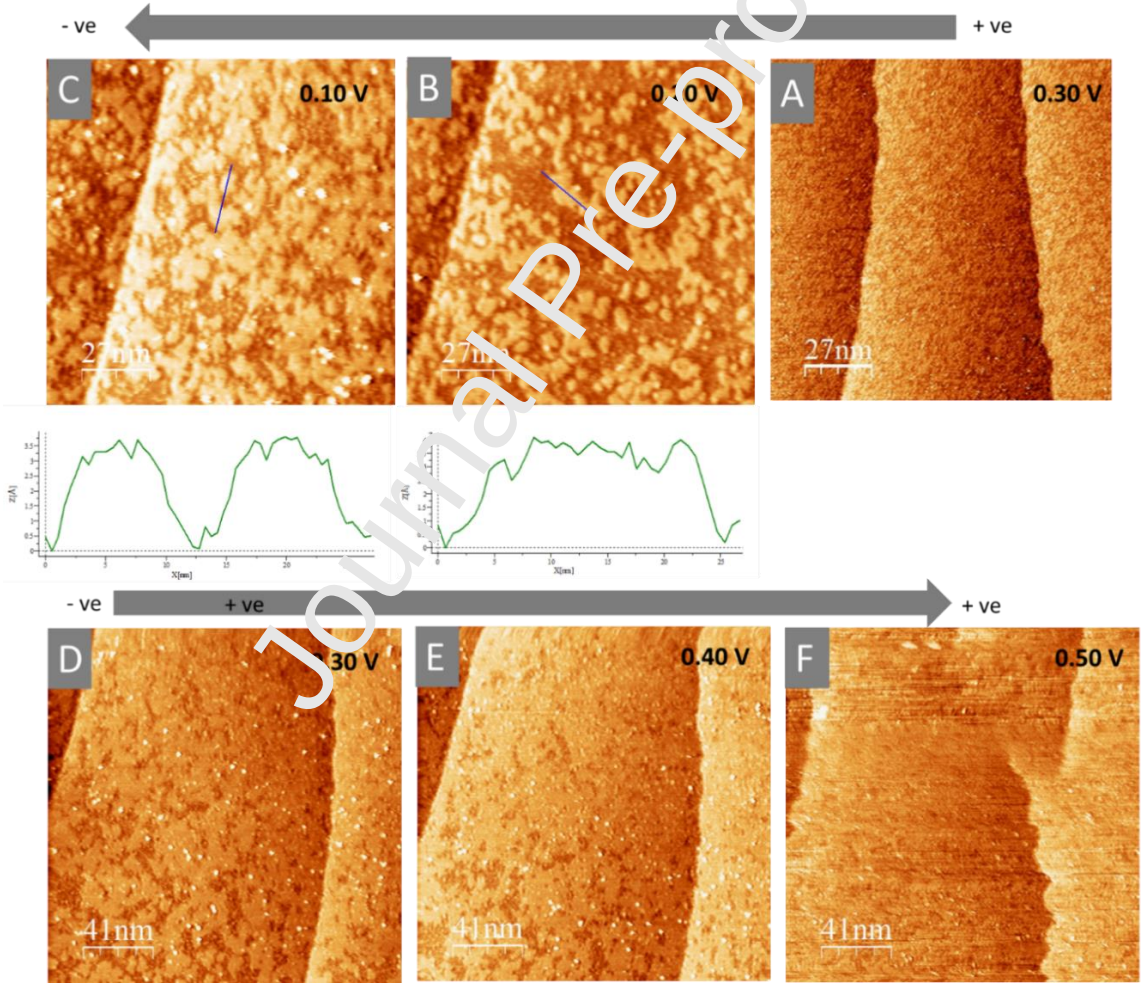

Figure 5. (A-C) In-situ STM images (135 x 135 nm^2) recorded during the sequential reduction of Ag^+ pre-adsorbed on cyanide-modified Pt(111) at E = 0.30 V (**A,** U_T = 0.10 V, tip negative), E = 0.20 V (**B**, U_T = 0.10 V, tip negative), and E = 0.10 V (**C**, U_T = 0.10 V, tip positive). **(D-F)** STM images (205 x 205 nm^2) recorded during the subsequent oxidation of the deposited Ag at E = 0.30 V (**D**, U_T = 0.10 V, tip negative), E = 0.40 V (**E**, U_T = 0.20 V, tip negative) and E = 0.50 V (**F**, U_T = 0.30 V, tip negative). All images acquired at tunnel current, I_T = 2 nA. The height profiles shown below images **(B)** and **(C)** correspond to those along the blue lines in the corresponding images.

Figs. 5 A, B and C illustrate images successively acquired in the direction of the arrow from positive to more negative potentials at 0.30, 0.20 and 0.10 V. The image at 0.30 V shows no significant change as compared with the image acquired at 0.40 V, except for an increased contrast of the atomic-scale features within the terrace, which we were unable to image with a higher resolution. However, at 0.20 V bidimensional islands with an apparent height of 0.4 nm emerge. These islands are spread across the terraces and step edges, with a slight preference for nucleation on the top side of monoatomic steps, and we attribute them to one-atom high heteroepitaxial islands of Ag on the Pt(111) substrate. While a height of ca. 0.30 nm would be expected, STM images are a convolution of both topography and local tunneling barrier, and the difference between the work functions of Ag and Pt contributes to the apparent increased height of the bidimensional Ag Islands. It is worth noting that the islands cover more than 16% of the surface, whereas the maximum possible coverage by Ag^+ in the honeycomb structure shown in Fig. 3 is 0.16 ML. Therefore, the bidimensional islands in Fig. 5 cannot correspond to pure Ag, whether on or underneath the cyanide adlayer.

At 0.10 V (Fig. 5 C), the surface coverage by the bidimensional islands increases, as does the interconnectivity between them. At the same time, the apparent height of the islands decreases to ca. 0.35 nm, closer to that expected from purely geometrical considerations. Considering that the coverage of Ag^+ coordinated on the CN_{ad} is at most 0.16 ML, a coverage of the Pt(111) by bidimensional Ag islands beyond that limit is not possible. The clearly higher coverage observed in Fig. 5 C at 0.10 V must therefore be due to the formation of a AgPt surface alloy and concomitant Pt enrichment. This is in agreement with the assignment of the peak at 0.20 V in the corresponding CV (see Fig. 1) to the adsorption of hydrogen on a AgPt alloy containing more than 50% Ag. The decrease in the apparent height from 0.4 nm at 0.20 V to 0.35 nm at 0.10 V is consistent with an increase of the Pt content in the surface alloy. The formation of the AgPt surface alloy in the hydrogen adsorption region, as well as the enrichment in Pt at the most negative potential, must be caused by the surface diffusion of Pt into the islands from the steps and from underneath the Ag islands (and the concomitant diffusion of Ag into the surface of Pt). The increased diffusion at more negative potentials might be the result of the stronger adsorption of hydrogen on Pt, as compared to Ag. Also observed in the image at 0.10 V in Fig. 5 C is the emergence of bright spots preferentially deposited on the AgPt alloy bidimensional islands that we attribute to Pt clusters 0.6 – 0.7 nm in height and composed of 4-5 atoms. The observation of similar clusters during AgPt alloy formation has been previously reported [28,29], and attributed to the very narrow miscibility region of Ag and Pt. The platinum clusters are generated by displacement from the surface and subsequent deposition onto the Ag islands. Due to the very strong bond between the Pt atoms on the surface and adsorbed cyanide, we find it unlikely that all these processes result in the stripping of the cyanide adlayer and suggest that the processes described above result in a PtAg surface alloy buried under the cyanide adlayer. This is consistent with the evolution of the voltammetric profile described in the previous section. As discussed there, only when the potential is scanned beyond 1.1 V partial oxidative stripping of CN_{ad} occurs.

Figs. 5 D-F show STM images acquired after Ag deposition and surface alloy formation at 0.1 V (see Fig. 5 D), with an arrow indicating the sequence of imaging from negative to positive potentials. A potential step from 0.10 V to 0.30 and then 0.40 V results in a decrease of contrast and an increase of the surface coverage by the higher contrast features. We attribute this to an increase of Pt concentration in the AgPt surface alloy as some Ag is dissolved and attached again as Ag^+ to the cyanide layer (see discussion on the voltammetric profile in section 3.1), leading to a more homogenous composition of the electrode surface. A significant change is observed upon excursion to 0.50 V (Fig. 5 F), which results in a fuzzy image with wavelike step edges. As discussed in the section 3.1, the peak at 0.34 V in the CV of Fig. 1

cannot correspond to dissolution of Ag as Ag^+ into the aqueous solution and is therefore attributed to the oxidation of Ag to yield Ag^+ coordinated on the cyanide adlayer. The noisy appearance of the image at 0.50 V (Fig. 5 F) can be explained by the high mobility of the Ag^+ ions coordinated to the cyanide adlayer at low coverage. Please note that, even with the higher initial coverage, the STM images become noisy around 0.50 V (Fig. 4), which we have attributed to an increased mobility of Ag^+ ions adsorbed on the cyanide adlayer due to the release at sufficiently negative potentials of sulphate in Ag^+-sulphate ion pairs.

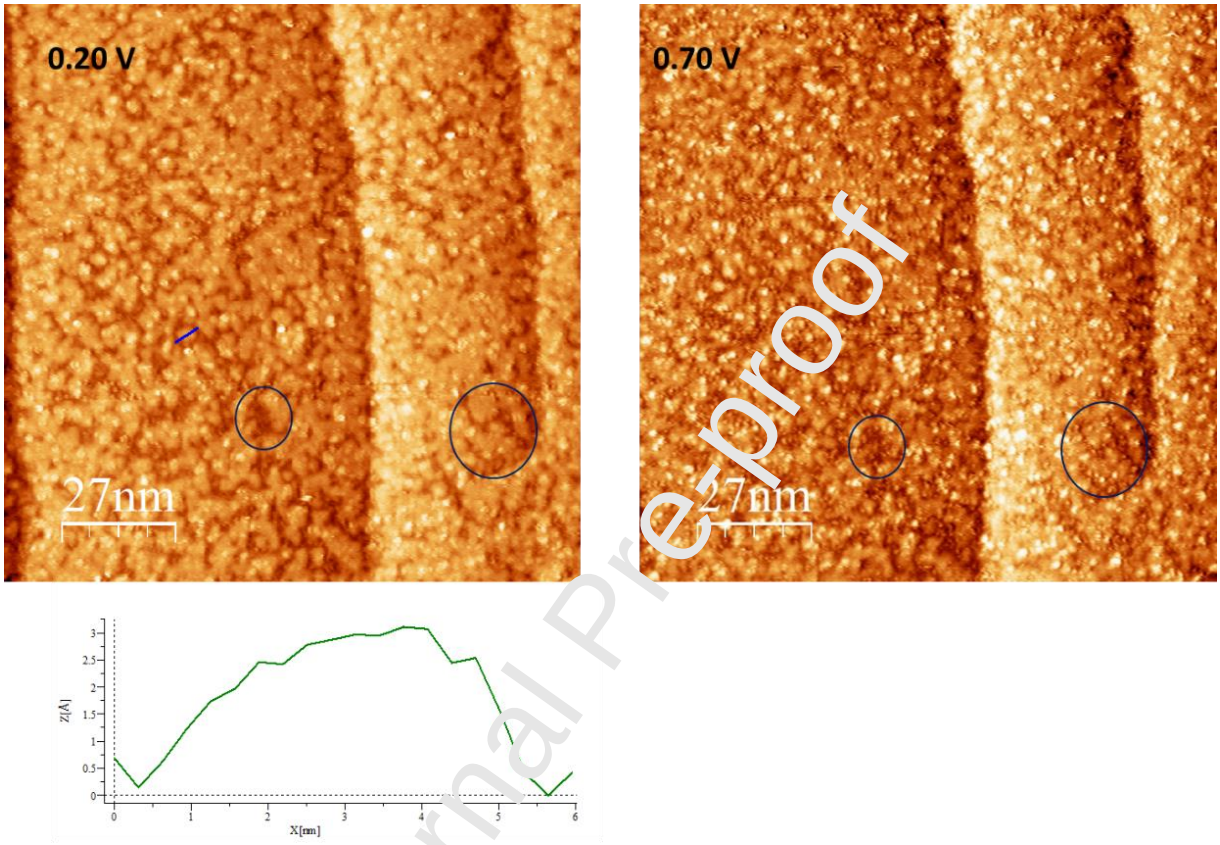

Figure 6. In situ STM images (135 x 135 nm^2) corresponding to the steady state achieved after repetitive potential cycling in Ag^+-free 0.1 M H_2SO_4. Left: at E = 0.20 V, (U_T = 0.50 V, tip negative); Right: at E = 0.70 V after a potential excursion to 1.0 V (U_T = 0.50 V, tip negative). Both images acquired at tunnelling current, I_T = 2 nA. The height profile on the left corresponds to the blue line across the island in the corresponding image. Blue circles of different sizes highlight the same areas in both images.

Fig. 6 shows STM images acquired once the steady-state CV has been obtained after repetitive cycling between 0.05 and 0.9 V. At 0.20 V the surface is covered by an interweaved pattern with an apparent height difference of 0.3 nm between high and low contrast areas, clearly smaller than that of similar features observed immediately after the first deposition of Ag (0.4 nm, see Fig. 5 C). As discussed above, we attribute the lower contrast to a lower Ag content in the AgPt surface alloy formed upon deposition. The interweaved pattern is due to the very narrow miscibility gap of Ag and Pt, which results in a tendency to phase separation into Pt- and Ag-rich areas, as observed in other surface alloy systems [33,34]. An image of the same area acquired at 0.70 V after excursion to 1.0 V shows that, although the contrast between brighter and darker areas has decreased, the shape of the features has barely changed at all (see, *e.g.*, blue circled areas in Fig. 6). There is also an increase in the number of small brighter spots, the height of which roughly corresponds to two atomic layers. This suggests that, even at the positive potential limit of the CV, part of the Ag in the surface alloy remains in the surface. A similar

behaviour has been reported by Beckord et al. during the dealloying of AgPt surface alloys [28], and was attributed to the strong lateral ligand effects contributed by the neighbouring Pt atoms, which results in the stabilization of the surface alloy.

In summary, successive potential cycling of Ag^+ preadsorbed on a cyanide modified Pt(111) results in Ag deposit on the Pt substrate. The Ag deposit forms a AgPt surface alloy at potentials negative of 0.2 V. Partial reoxidation of some of the Ag in the surface alloy to yield Ag^+ adsorbed on the remaining cyanide adlayer is observed at 0.34 V. As only part of the deposited Ag is oxidized in this process, the corresponding charge density diminishes with successive potential cycling. When the positive potential limit is extended to 1.2 V, some of the Ag is released as Ag^+ into the bulk of the solution and the cyanide adlayer is partially stripped. In comparison, repeated potential cycling for long periods of a polycrystalline platinum in a Ag^+-containing solution also results in the formation of an AgPt alloy [35]. In the case of Pt(111) in Ag^+ containing solution, a layer by layer growth of Ag deposition followed by formation of Ag clusters has been reported [36,37]. The Ag clusters have been demonstrated to subsequently form an AgPt alloy upon annealing at 620 K [36]. This is in contrast with our observation of AgPt surface alloy formation on Pt(111) upon repeated potential cycling in a solution containing no Ag^+ and at room temperature.

8 Conclusion

We have attempted the metallization of cyanide-modified Pt(111) electrodes by reducing pre-adsorbed Ag^+ in Ag^+-free sulphuric acid. By combining cyclic voltammetry and in-situ STM, we have shown that, above 0.70 V, Ag^+ adsorbs irreversibly on the cyanide adlayer forming a honeycomb structure, similar to that previously reported with preadsorbed Cu^{2+} [22], as well as in solutions containing alkaline-metal cations [20]. We have also shown that reduction of the pre-adsorbed Ag^+ ions results in the deposition of Ag on the Pt(111) substrate. This reduction, and the subsequent reoxidation to yield Ag^+ coordinated to CN_{ad}, occurs at a potential much more negative than expected from the standard potential of the Ag^+/Ag couple, which can be attributed to the increased stability of the oxidized form of the couple due to its interaction with CN_{ad}.

Ag deposition is followed by the formation of AgPt surface alloy. The formation of AgPt alloy on Pt(111) in Ag^+ free solution at ambient conditions is enabled by the strong interaction of the adsorbed cyanide with Ag and/or Pt, which possibly increases their surface mobility enabling their intermixing. We recently reported [23] that the reduction of Pd^{2+} preadsorbed on cyanide-modified Pt(111) also results in the direct deposition of Pd onto the Pt substrate, but no alloy formation was detected in that case, which is interesting considering the similitude between the lattice parameters of Pd and Pt (3.86 and 3.92 Å respectively) and the relatively larger difference in the case of Ag and Pt (4.08 and 3.92 Å respectively).

References

[1] H. Hagenström, M.A. Schneeweiss, D.M. Kolb, Copper underpotential deposition on ethanethiol-modified Au(111) electrodes: kinetic effects, Electrochim. Acta. 45 (1999) 1141–1145. https://doi.org/http://dx.doi.org/10.1016/S0013-4686(99)00314-X.

[2] M. Nishizawa, T. Sunagawa, H. Yoneyama, Underpotential Deposition of Copper on Gold Electrodes through Self-Assembled Monolayers of Propanethiol, Langmuir 13 (1997). https://doi:10.1021/la970545f

[3] O. Cavalleri, A.M. Bittner, H. Kind, K. Kern, Copper Electrodeposition on Alkanethiolate Covered

Gold Electrodes, Zeitschrift Phys. Chemie. 208 (1999) 107–136. https://doi.org/doi:10.1524/zpch.1999.208.Part_1_2.107.

[4] S.E. Gilbert, O. Cavalleri, K. Kern, Electrodeposition of Cu Nanoparticles on Decanethiol-Covered Au(111) Surfaces: An in Situ STM Investigation, J. Phys. Chem. 100 (1996) 12123–12130. doi:10.1021/jp960053w.

[5] M.A. Schneeweiss, H. Hagenström, M.J. Esplandiu, D.M. Kolb, Electrolytic metal deposition onto chemically modified electrodes, Appl. Phys. A. 69 (1999) 537–551. doi:10.1007/s003390051465.

[6] D. Oyamatsu, S. Kuwabata, H. Yoneyama, Underpotential deposition behavior of metals onto gold electrodes coated with self-assembled monolayers of alkanethiols, J. Electroanal. Chem. 473 (1999) 59–67. doi:10.1016/S0022-0728(99)00104-7.

[7] T. Baunach, V. Ivanova, D.M. Kolb, H.G. Boyen, P. Ziemann, M. Büttner, P. Oelhafen, A New Approach to the Electrochemical Metallization of Organic Monolayers: Palladium Deposition onto a 4,4'-Dithiodipyridine Self-Assembled Monolayer, Adv. Mater. 16 (2004) 2024–2028. doi:10.1002/adma.200400409.

[8] O. Shekhah, C. Busse, A. Bashir, F. Turcu, X. Yin, P. Cyganik, A. Birkner, W. Schuhmann, C. Woll, Electrochemically deposited Pd islands on an organic surface: the presence of Coulomb blockade in STM I(V) curves at room temperature, Phys. Chem. Chem. Phys. 8 (2006) 3375–3378. doi:10.1039/B606488D.

[9] C. Silien, D. Lahaye, M. Caffio, R. Schaub, N.R. Champness, M. Buck, Electrodeposition of Palladium onto a Pyridine-Terminated Self-Assembled Monolayer, Langmuir. 27 (2011) 2567–2574. doi:10.1021/la104561j.

[10] M.I. Muglali, J. Liu, A. Bashir, D. Borissov, M. Xu, Y. Wang, C. Wöll, M. Rohwerder, On the complexation kinetics for metallization of organic layers: palladium onto a pyridine-terminated araliphatic thiol film, Phys. Chem. Chem. Phys. 14 (2012) 4703–4712. doi:10.1039/c2cp40072c.

[11] D. Qu, K. Uosaki, Electrochemical Metal Deposition on Top of an Organic Monolayer, J. Phys. Chem. B. 110 (2006) 17570–17577. doi:10.1021/jp0632135.

[12] M. Manolova, V. Ivanova, D.M. Kolb, H.G. Boyen, P. Ziemann, M. Büttner, A. Romanyuk, P. Oelhafen, Metal deposition onto thiol-covered gold: Platinum on a 4-mercaptopyridine SAM, Surf. Sci. 590 (2005) 146–153. doi:10.1016/j.susc.2005.06.005.

[13] F. Eberle, M. Saitner, H.G. Boyen, J. Kucera, A. Gross, A. Romanyuk, P. Oelhafen, M. D'Olieslaeger, M. Manolova, D.M. Kolb, A molecular double decker: Extending the limits of current metal-molecule hybrid structures, Angew. Chemie Int. Ed. 49 (2010) 341–345. doi:10.1002/anie.200905339.

[14] J.A. Mwanda, A. Cuesta, Electrochemical metallization of molecular adlayers, Curr. Opin. Electrochem. 17 (2019) 72–78. doi:10.1016/j.coelec.2019.04.022.

[15] C.S. Kim, C. Korzeniewski, Cyanide adsorbed as a monolayer at the low-index surface planes of platinum metal electrodes: an in situ study by infrared spectroscopy, J. Phys. Chem. 97 (1993) 9784–9787. doi:10.1021/j100140a041.

[16] C. Stuhlmann, I. Villegas, M.J. Weaver, Scanning tunneling microscopy and infrared spectroscopy as combined in situ probes of electrochemical adlayer structure. Cyanide on Pt(111), Chem. Phys. Lett. 219 (1994) 319–324. doi:10.1016/0009-2614(94)87064-0.

[17] V.B. Paulissen, C. Korzeniewski, Infrared spectroscopy as a probe of the adsorption and electrooxidation of a cyanide monolayer at platinum under aqueous electrochemical conditions, J. Phys. Chem. 96 (1992) 4563–4567. doi:10.1021/j100190a079.

[18] M. Escudero-Escribano, G.J. Soldano, P. Quaino, M.E. Zoloff Michoff, E.P.M. Leiva, W. Schmickler,

Á. Cuesta, Cyanide-modified Pt(111): Structure, stability and hydrogen adsorption, Electrochim. Acta. 82 (2012) 524–533. doi:10.1016/j.electacta.2012.02.062.

[19] M. Escudero, A. Cuesta, Electrocatalysis and Surface Nanostructuring : Atomic Ensemble Effects and Non-Covalent Interactions, Universidad Autónoma de Madrid, 2011. http://hdl.handle.net/10261/42378.

[20] M. Escudero-Escribano, M.E. Zoloff Michoff, E.P.M. Leiva, N.M. Marković, C. Gutiérrez, A. Cuesta, Quantitative Study of Non-Covalent Interactions at the Electrode-Electrolyte Interface Using Cyanide-Modified Pt(111) Electrodes, ChemPhysChem. 12 (2011) 2230–2234. doi:10.1002/cphc.201100327.

[21] M. Escudero, J.F. Marco, A. Cuesta, Surface Decoration at the Atomic Scale Using a Molecular Pattern: Copper Adsorption on Cyanide-Modified Pt(111) Electrodes, J. Phys. Chem. C. 113 (2009) 12340–12344. doi:10.1021/jp901643q.

[22] M. Escudero-Escribano, C. Wildi, J.A. Mwanda, A. Cuesta, Metallization of cyanide-modified Pt(111) electrodes with copper, J. Solid State Electrochem. 20 (2016) 1087–1094. doi:10.1007/s10008-015-2968-7.

[23] J.A. Mwanda, A. Cuesta, Reduction of Pd^{2+} pre-adsorbed on cyanide-modified Pt(111) electrodes: Adlayer metallization vs. metal-on-metal deposition, Electrochim. Acta. 292 (2018) 419–424. doi:10.1016/j.electacta.2018.08.120.

[24] J. Clavilier, R. Faure, G. Guinet, R. Durand, Preparation of monocrystalline Pt microelectrodes and electrochemical study of the plane surfaces cut in the direction of the {111} and {110} planes, J. Electroanal. Chem. 107 (1979) 205–209. doi:10.1016/S0022-0728(79)80022-4.

[25] C. Wildi, G. Cabello, M.E. Zoloff Michoff, P. Vélez, E.P.M. Leiva, J.J. Calvente, R. Andreu, A. Cuesta, Super-Nernstian Shifts of Interfacial Proton-Coupled Electron Transfers: Origin and Effect of Noncovalent Interactions, J. Phys. Chem. C. 120 (2016) 15586–15592. doi:10.1021/acs.jpcc.5b04560.

[26] F. Huerta, E. Morallón, J. Vázquez, Voltammetric analysis of the co-adsorption of cyanide and carbon monoxide on a Pt(111) surface, Electrochem. Commun. 4 (2002) 251–254. doi:10.1016/S1388-2481(02)00271-0.

[27] I. Morales-Moreno, A. Cuesta, C. Gutierrez, Accurate determination of the CO coverage at saturation on a cyanide-modified Pt(111) electrode in cyanide-free 0.5 M H2SO4, J. Electroanal. Chem. 560 (2003) 135–141. doi:10.1016/j.jelechem.2003.07.008.

[28] S. Beckord, A.K. Engstfeld, S. Brimaud, R.J. Behm, Electrochemical Characterization and Stability of Ag_xPt_{1-x}/Pt(111) Surface Alloys, J. Phys. Chem. C. 120 (2016) 16179–16190. doi:10.1021/acs.jpcc.6b00528.

[29] S. Beckord, S. Brimaud, R.J. Behm, Stability and ORR performance of a well-defined bimetallic $Ag_{70}Pt_{30}$/Pt(111) monolayer surface alloy electrode – Probing the de-alloying at an atomic scale, Electrochim. Acta. 259 (2018) 762–771. doi:10.1016/J.ELECTACTA.2017.10.146.

[30] F. Huerta, F. Montilla, E. Morallón, J.L. Vázquez, On the vibrational behaviour of cyanide adsorbed at Pt(111) and Pt(100) surfaces in alkaline solutions, Surf. Sci. 600 (2006) 1221–1226. doi:10.1016/j.susc.2005.12.046.

[31] F. Huerta, E. Morallón, J.L. Vázquez, Structural effects of adsorbed CN adlayers on the co-adsorption of OH− at the Pt(111) surface in sulfuric acid medium, Surf. Sci. 431 (1999) L577–L581. https://doi.org /10.1016/S0039-6028(99)00580-4.

[32] Y.-G. Kim, S.-L. Yau, K. Itaya, Direct Observation of Complexation of Alkali Cations on Cyanide-Modified Pt(111) by Scanning Tunneling Microscopy, J. Am. Chem. Soc. 118 (1996) 393–400.

doi:10.1021/ja9521841.

[33] A.K. Engstfeld, H.E. Hoster, R.J. Behm, Formation, atomic distribution and mixing energy in two-dimensional Pd_xAg_{1-x} surface alloys on Pd(111), Phys. Chem. Chem. Phys. 14 (2012) 10754. doi:10.1039/c2cp41104k.

[34] H.E. Hoster, A. Bergbreiter, P.M. Erne, T. Hager, H. Rauscher, R.J. Behm, Pt_xRu_{1-x}/Ru(0001) surface alloys—formation and atom distribution, Phys. Chem. Chem. Phys. 10 (2008) 3812. doi:10.1039/b802169d.

[35] P. Ocón, P. Herrasti, C. Palacio, M.E. Vela, R.C. Salvarezza, L. Vazquez, A. Arvia, The role of slow surface-atom reordering processes in the underpotential deposition of metals Silver underpotential deposition on platinum in acid solutions, J. Electroanal. Chem. 357 (1993) 339–355. https:// doi:10.1016/0022-0728(93)80390-4

[36] H. Röder, R. Schuster, H. Brune, K. Kern, Monolayer-Confined Mixing at the Ag-Pt(111) Interface, Phys. Rev. Lett. 71 (1993) 2086–2091. https:// doi:10.1103/PhysRevLett.71.2086

[37] H. Röder, H. Brune, J.-P. Bucher, K. Kern, Changing morphology of metallic monolayers via temperature controlled heteroepitaxial growth, Surf. Sci. 298 (1993) 121–126. doi:10.1016/0039-6028(93)90088-2.